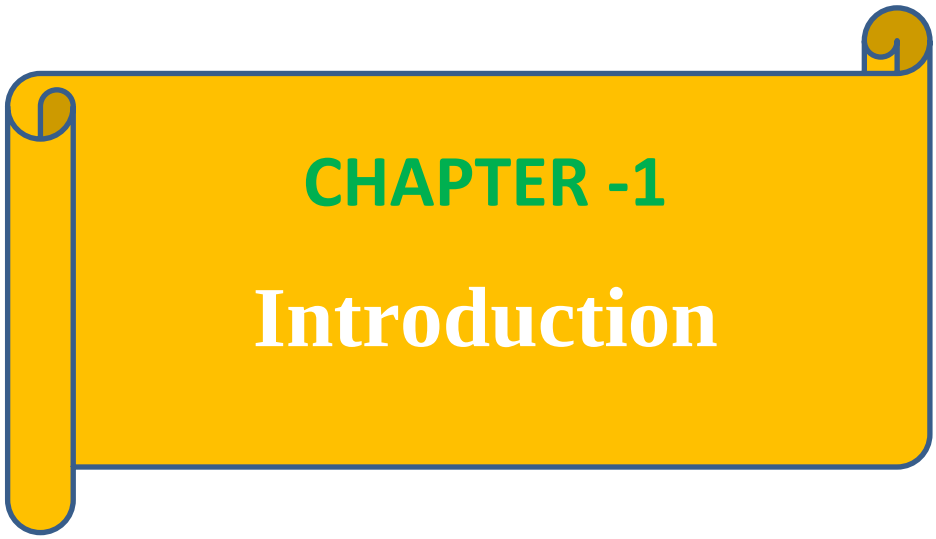
CHAPTER -1
Introduction

1.1 Superalloys

Superalloys are high performance heat resistant alloys, which exhibit excellent strength and oxidation resistance at elevated temperatures. These alloys can withstand loads for extended durations even at service temperatures close to melting point of the alloys without mechanical degradation. Generally, these alloys contain nickel, cobalt, or iron in the matrix in which various other alloying elements are added for strengthening. Addition of tungsten, molybdenum, tantalum and niobium provide solution strengthening whereas addition of elements like as titanium and aluminium impart precipitation strengthening to these alloys. The unique feature of these superalloys is that they possess good mechanical properties, resistance to oxidation and corrosion along with excellent microstructural stability at elevated temperatures which make these alloys superior to other competitive materials such as ceramics and refractory metal alloys for high temperature applications [1]. Development of commercial gas turbine engines for aircraft and land based applications mandated the emergence of many complex superalloys and the diverse microstructural features of these alloys allowed the development of a wide range of alloys which can be optimized through processing for specific applications.

Wide varieties of superalloys devoted to specific applications have been developed and studied in detail by various researchers. The need for materials with higher-temperature capability has taken the development of superalloys to the high level of sophistication [2]. Refractory metals can sustain high temperatures due to their high melting points, but the poor oxidation resistance and ductility limit their usage in many applications compared to those of superalloys. Similarly, despite having excellent oxidation and corrosion resistance, ceramic materials also cannot meet the requirements of the intended applications due to their poor toughness and ductility [3].

1.2 Classification of Superalloys

Superalloys can be broadly classified based on the major element present in the alloys as: 1. Iron-based superalloys 2. Nickel-based superalloys and 3. Cobalt-based superalloys. Fig. 1.1 gives the major classification of different superalloys and some examples of commercially available superalloys for different applications. Iron based superalloys contain iron as the main element with minimum 25% nickel content to stabilise the austenitic matrix. Other alloying elements are added to impart solid solution as well as precipitation strengthening. These alloys are less expensive than the other two categories of superalloys. Nickel based superalloys are discussed in detail in the next section (section 1.3) as the superalloy Inconel 617 is of interest for the present study.

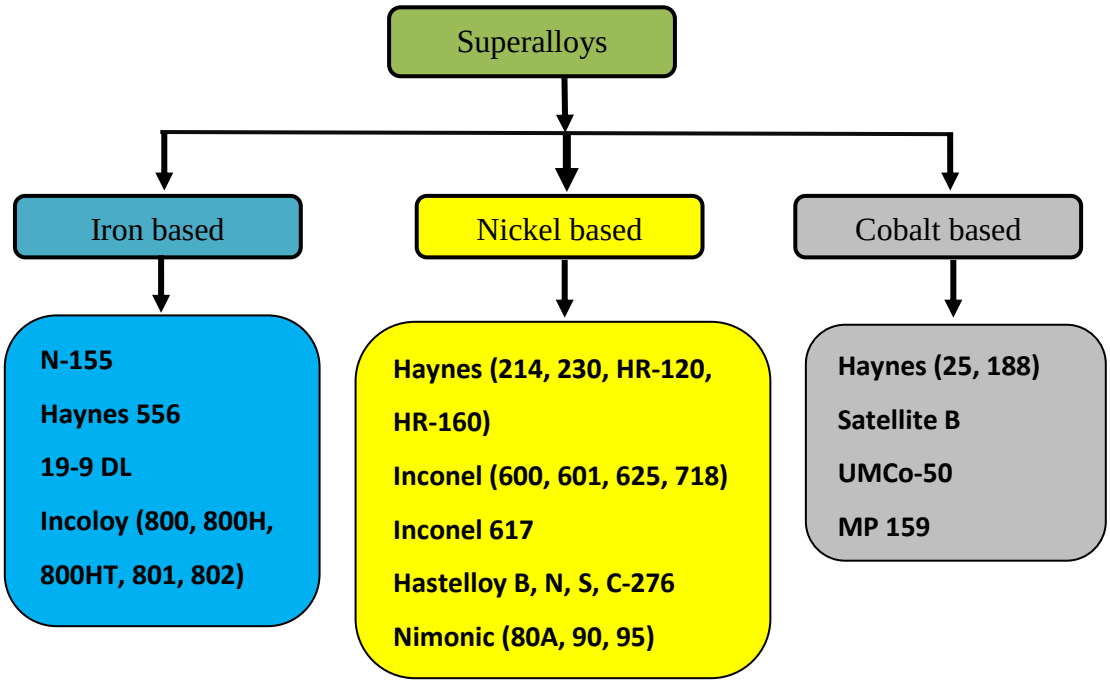

Fig 1.1: Major classification and designation of important superalloys.

Cobalt based superalloys can be used in the applications where the temperatures reach as high as 1100^{o}C where nickel based alloys cannot sustain such high

temperatures. Strengthening of these alloys is based on the precipitation of carbides of refractory elements such as Mo and W along the grain boundaries. These are expensive than the nickel based superalloys and hence used in critical parts where the requirement substantiates the cost [4].

1.3 Nickel-based Superalloys

Nickel-based superalloys are special class of superalloys which contain nickel as the main element which stabilises the austenitic (*fcc*) matrix and combination of other alloying elements such as chromium (10-25%), cobalt (5-15%), molybdenum (around 10%), aluminium and titanium (up to 8% combined) for improving high temperature properties. Tungsten and niobium are also added to these alloys in some cases to provide solution strengthening and formation of carbides. These are complex and have wide range of critical applications among the three categories and the most interesting alloys for metallurgists. The alloys were developed in 1940s for jet engines in aircrafts where the requirement of materials with good creep strength and stress rupture strength are desired [5]. Increase in the operating temperature of jet engines increase the speed of the engines, which increase the demand for high heat resistant materials. This contributed to the complementary advancement of both the jet engine technology and the development of new nickel based superalloys [6].

There is no standard system for designation of the nickel based superalloys. Nimonic, Incoloy, Inconel, Hastelloy and Rene are some of the families of nickel based alloys. Superalloys can be polycrystalline, columnar grained or single crystal depending on the fabrication route adopted. All these superalloys can be categorised into conventionally cast, single crystal and directionally solidified superalloys. Table 1.1 gives the list of popular and commercially available nickel based polycrystalline

superalloys along with their compositions.

Table 1.1: Various Nickel-based Superalloys [3].

Alloy	Ni	Fe	Cr	Mo	W	Co	Nb	Al	C	Others
Astroloy	55.0	--	15.0	5.3	--	17.0	--	4.0	0.06	--
Nimonic 75	75.0	2.5	19.5	--	--	--	--	0.15	<0.08	1 V
Hastelloy X	49.0	18.5	22.0	9.0	0.6	1.5	3.6	2.0	0.10	--
Inconel 625	61.0	2.5	21.5	9.0	--	--	--	0.2	0.15	<0.25Cu
Inconel 617	Bal	<3.0	22.0	9.0	--	12.5	--	1.2	0.10	<0.6 Ti
Inconel 100	60.0	<0.6	10.0	3.0	--	15.0	--	5.5	<0.08	2.9 (Nb+Ta)
Inconel 706	41.5	37.5	16.0	--	--	--	5.1	0.2	0.12	<0.5Cu
Inconel 716	52.5	18.5	19.0	3.0	--	--	5.2	0.5	0.05	0.1 Zr
Inconel 792	61.0	3.5	12.4	1.9	3.8	9.0	--	3.5	0.04	--
Inconel 901	42.7	34.0	13.5	6.2	--	--	--	0.2	0.60	0.3 V
Rene 95	61.0	<0.3	14.0	3.5	3.5	8.0	--	3.5	0.40	--
Rene 104	52.0	--	13.1	3.8	1.9	18.2	1.4	3.5	0.03	2.7 Ta
SXPWA1480	64.0	--	10.0	--	4.0	5.0	--	5.0	--	2 Hf
DSPWA1422	60.0	--	10.0	--	12.5	10.0	--	5.0	--	--

1.3.1 Development of Nickel-based Superalloys

Turbine blades are being made from single crystal nickel-based superalloys for many years. The first generation of superalloys were introduced in early 1950s [6] and were focussed mainly on improving high temperature strength by additions of γ′ [Ni_3(Ti, Al)] formers which eliminate the deleterious phases and improve castability. The first generation of single crystal superalloys did not contain rhenium. CMSX-2 and Rene N4 are examples for this generation of alloys. Second generation single crystal super alloys were developed in the late 1980s and are often used in both commercial and military aircraft engines. These alloys typically contain 3% rhenium (Re) by

weight, which distinguish them from first generation single crystal super alloys. Increase in percentage of refractory element, Re and γ′ formers by more than 6% was achieved in this generation of superalloys. Examples of second generation alloys include Rene N5, CMSX-4 and PWA 1484.

Third generation alloys were designed to increase the temperature capability and creep resistance further, by increasing Re addition to ~6 wt% though there was reduction in chromium content levels. These contained hafnium (Hf). Examples of these alloys include Rene N6, CMSX-10 and DMS4. A fourth generation of superalloys developed later which contain platinum group elements mainly Rhuthenium (Ru). EPM 102 is example of this generation which has more phase stability and higher strength than those of earlier alloys. The fourth generation alloy EPM 102 is about 6% heavier than second generation alloys. TMS 138 is also an example for this generation of super alloys. Later generation alloys had high alloy densities which limited the use of the superalloys, and hence third and fourth generation alloys are used only in specialized applications. Fifth generation of alloys included Ru greater than 6 wt% to achieve the desired structure. In 2008, two fifth generation nickel-based single crystal super alloys, TMS-162 and TMS-172, were developed in Japan. Both alloys were seen to exhibit excellent creep resistance. Sixth generation alloy TMS-238 was developed by National institute for materials science [NIMS], Japan. The reduction of the Mo and W contents and increase in the contents the Co and Ta in this alloy improved oxidation and hot corrosion resistance [7].

1.3.2 Physical Metallurgy of Nickel-based Superalloys

There are four different major phases that occur in nickel-based super alloys [8]:

1. Gamma (γ)

2. Gamma Prime (γ')
3. Gamma double prime (γ'')
4. Carbides
5. Topologically Close-Packed Phases

1. Gamma (γ): The matrix (called gamma) is a nickel-based austenitic phase with face-centered-cubic (*fcc*) crystal structure. Elements such as Co, Cr, Mo, and W, provide solid solution strengthening of the γ.

2. Gamma Prime (γ'): This is the primary precipitation strengthening phase in these alloys. Generally Ti or Al elements act as **γ'** formers which constitute Ni_3Al or Ni_3Ti phase. It is a coherent precipitate with cube on cube orientation relationship with the matrix. And the crystal structure is ordered *fcc* crystal structure as shown in Fig.1.2.

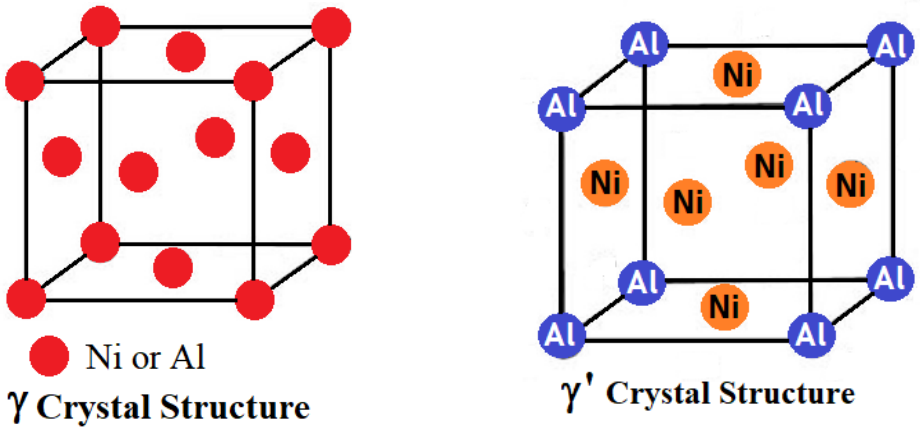

Fig. 1.2 Crystal structure of γ and γ' in nickel based superalloys.

3. Gamma double prime (γ''): This is body center tetragonal (BCT) phase of Ni_3Nb and coherent with the γ matrix, which is unstable above 650°C. This phase exists only in the presence of Nb in the Ni-Fe alloys. This phase provides high strength at intermediate range of temperatures (450-750°C).

4. Carbides: Carbides form in these alloys due to the carbon present in the range of 0.05-0.2%, which combines with carbide forming elements such as chromium, molybdenum, titanium, tantalum, and hafnium. These carbides (MC) decompose on subjecting the alloy to heat treatment or during service to form other carbides such as $M_{23}C_6$ and M_6C, which tend to form at the grain boundaries. The crystal structure of these carbides is *fcc* which is same as that of matrix. The stress rupture strength of nickel based superalloys at the elevated temperatures is enhanced due to the formation of these carbides along grain boundaries.

5. Topologically Close-Packed Phases (TCP): Phases like σ, μ and Laves phases etc. form during heat treatment or service which induce brittleness to the alloy and hence these phases are not desirable. Generally these TCPs form as plates and usually appear as needles at high magnifications. The other deleterious effect of TCPs is that they combine with **γ** and **γ'** strengthening elements to form deleterious phases and reduce creep strength of the alloy [9].

1.3.3 Applications of Nickel-based Superalloys

Though nickel based superalloys find their extensive applications in land based and aircraft based (commercial and military aircrafts) gas turbine engines, they are also used in some other important applications depending on their suitability. Table 1.2 gives the details of different applications of nickel based superalloys [10].

1.4 Nickel-based Superalloy Inconel 617

Inconel 617 is a nickel based solid solution strengthened superalloy, a candidate material for combustion liners in marine and land based gas turbine engines. Along with Ni, the alloy contains Cr, Co and Mo as other prime alloying elements. Co and Mo impart solid solution strengthening to the alloy. Al and Ti are also added in this alloy in

small quantities to form homogeneously dispersed fine γ′, which contribute to precipitation strengthening. Table 1.3 shows the standard chemical composition of the Inconel 617 alloy [11]. Precipitation of M_6C and $M_{23}C_6$ carbides also induce strengthening. Formation of strong oxide layers of Cr and Al makes this alloy highly resistant to oxidation and corrosion at elevated temperatures [12, 13].

Table 1.2: Various Applications of Nickel-based Superalloys.

Industry	Applications	Designation of candidate alloys
Aircraft Gas turbine engines	Vanes, blades, disks, shafts, combustion chambers, cases, bolts, thrust reversers, burner cans, after burners and exhaust systems	Inconel 718, Waspaloy, Nimonic 90, Inconel 617, Hastelloy X, Haynes 188, Inconel X750
Power plant machinery: steam turbines	Bolts, blades, stack gas re-heaters and super-heaters	Inconel 601, Inconel 617, Inconel 625, Inconel 718 Haynes 230, Inconel 740, Nimonic 263
Aerospace components	Rocket engine parts, Aerodynamically heated sinks	Alloy 601, Alloy X750, Alloy X
Reciprocating engines	Exhaust valves, valve seat inserts, turbochargers, hot plugs	Alloy X, Alloy X750
Nuclear power systems	Control rod drive mechanisms, valve stems, springs, ducting	Inconel 600 Alloy X750
Metal processing	Hot work tools, dies for hot work and casting	Alloy X750, Nimonic 90
Chemical and petrochemical industries	Fans, valves, reaction vessels, bolts, pumps, piping	Inconel 600, Inconel 617, Alloy 601

This alloy was developed in 1970s and has good resistance to pitting and crevice corrosion along with exceptional creep strength at temperatures above 850^{o}C [13]. It has good weldability and metallurgical stability as it does not form deleterious phases like σ, μ and χ at elevated temperatures. This tungsten free alloy is lighter and cost competitive compared to other nickel based alloys with tungsten [12]. This alloy has good formability at high temperatures though it requires comparatively large forming

stresses due to formation of carbides at high temperatures. The hot working or forging temperature range for this alloy is 1000 to 1200°C. Though work hardening rate is high for this alloy cold working can be performed using conventional methods. Annealing at 1040°C after cold working is required to homogenise the microstructure. Table 1.4 shows various physical properties of Inconel 617 alloy. Fig. 1.3 shows variation of mechanical properties with temperature for Inconel 617 alloy [11].

1.4.1 Heat Treatment of Inconel 617 Alloy

Inconel 617 alloy is generally used in the solution annealed condition which provides a coarse grain structure for better creep strength. This condition gives the alloy optimum strength with good ductility at room temperature. It also provides the best bend ductility at room temperature. The standard heat treatment cycle for solution annealing consists of subjecting the alloy to heating upto1175^{o}C and holding for specified time depending on the section size of the alloy which is followed by quenching in water or rapid cooling in the air [11].

Table 1.3: Standard Chemical Composition of the Inconel 617 Alloy [11].

Element	**Nickel**	**Chromium**	**Cobalt**	**Molybdenum**	**Aluminium**	**Titanium**
Weight %	44.5 min	20.0-24.0	10.0-15.0	8.0-10.0	0.8-1.5	0.6 max
Element	Carbon	Silicon	Iron	Manganese	Boron	Sulfur
Weight %	0.05-0.15	1.0 max	3.0 max	1.0 max	0.006 max	0.015 max

Table 1.4: Physical Properties of Inconel 617 [11].

Density gm/cc	8.36
Melting Range, ^{o}C	1332-1380
Super Heat at 26^{o}C, J/Kg-^{o}C	4192
Electric Resistivity at 26^{o}C, μΩ-m	1.22

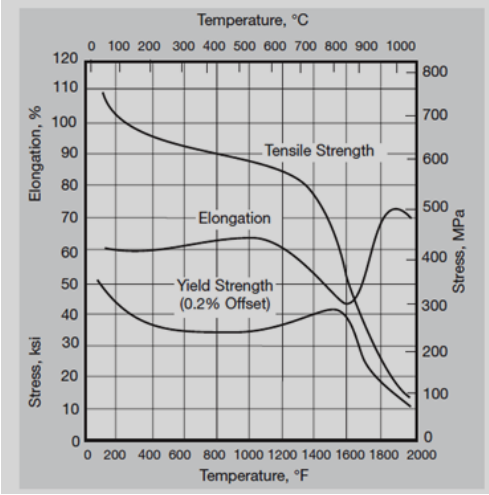

Fig. 1.3: Variation of tensile properties of Inconel 617 alloy with temperature [11].

1.4.2 Physical Metallurgy of Inconel 617 Alloy

The phases that form in this alloy are similar to that discussed in section 1.3.2, however no gamma double prime (γ″) and TCP phases form for this alloy in the composition range specified. Ti(C, N) is the additional phase that forms in this alloy during solidification or heat treatment and is stable even at room temperature. Phase transformation and phase stability in this alloy after subjecting this alloy to aging treatment after solution annealing treatment can be described by using time temperature transformation (TTT) diagram as reported by several researchers[3, 14, 15]. Fig. 1.4 shows TTT diagram of Inconel 617 alloy which indicates phases that form after aging treatment. Carbides and γ′ are the two main precipitate phases found in this alloy which vary with the duration of the aging.

Carbides: The reaction of various carbide forming elements with carbon in this alloy forms mainly three types of carbides namely MC, M_6C and $M_{23}C_6$ where M stands for carbide forming element (Cr, Mo, Co and Ti in this alloy). MC carbides form during solidification of the alloy, without any orientation relationship with the matrix and mostly heterogeneous or randomly exist within grains and along grain boundaries. MC

has *fcc* crystal structure. These carbides are generally coarse in size and exhibit script morphology. TiC is the main carbide stable at room temperature though less in fraction. Other MC carbides transforms to $M_{23}C_6$ and M_6C carbides during heat treatment or processing. This transformation may also take place during service. M_6C carbides generally transform from MC carbides in the temperature range of 815^{o}C to 980^{o}C during heat treatment or processing. These are generally molybdenum rich carbides and exists in form of $(Ni,Co)_3 Mo_3C$. These are important carbides at higher temperature for grain boundary strengthening. These carbides are stable at higher temperature than $M_{23}C_6$ carbides and have complex cubic structure.

$M_{23}C_6$ carbides are chromium rich carbides like $Cr_{23}C_6$, and form at low temperature range than that for M_6C carbides. These carbides originate from the residual carbon in the solid solution or by transformation from the MC carbides. These carbides maintain cube on cube orientation relationship with the matrix as both have *fcc* crystal structure. These carbides generally exist as either $Cr_{23}C_6$ or $Cr_{21}Mo_2C_6$. Sometimes nickel or cobalt may replace chromium to form complex carbides. These carbides are normally found along grain boundaries and inhibit grain boundary sliding which increases the creep rupture strength of this alloy at elevated temperatures, hence these are important phases compared to other phases in this alloy. However, these carbides act as nucleation sites for void formation as they come out of the matrix due to decohesion under loading and causes premature failure of the material which can be avoided by proper heat treatment.

Gamma prime (γ′): This phase is an intermetallic phase compound with *fcc* crystal structure. This phase also exhibits orientation relationship with the matrix. Generally this phase is in the form of Ni_3Al or Ni_3Ti and widely referred as $Ni_3(Ti, Al)$ phase. This has spherical shape morphology and is uniformly distributed throughout the matrix

though volume fraction of this phase is very less in this alloy due to very low concentration of Al and Ti. The morphology of the γ′ decides the mismatch fit with the matrix as plate like morphology exhibits high mismatch fit around 1.25% whereas sphere shape exhibits low mismatch fit around 0–0.2% while cuboidal shape exhibits intermediate range.

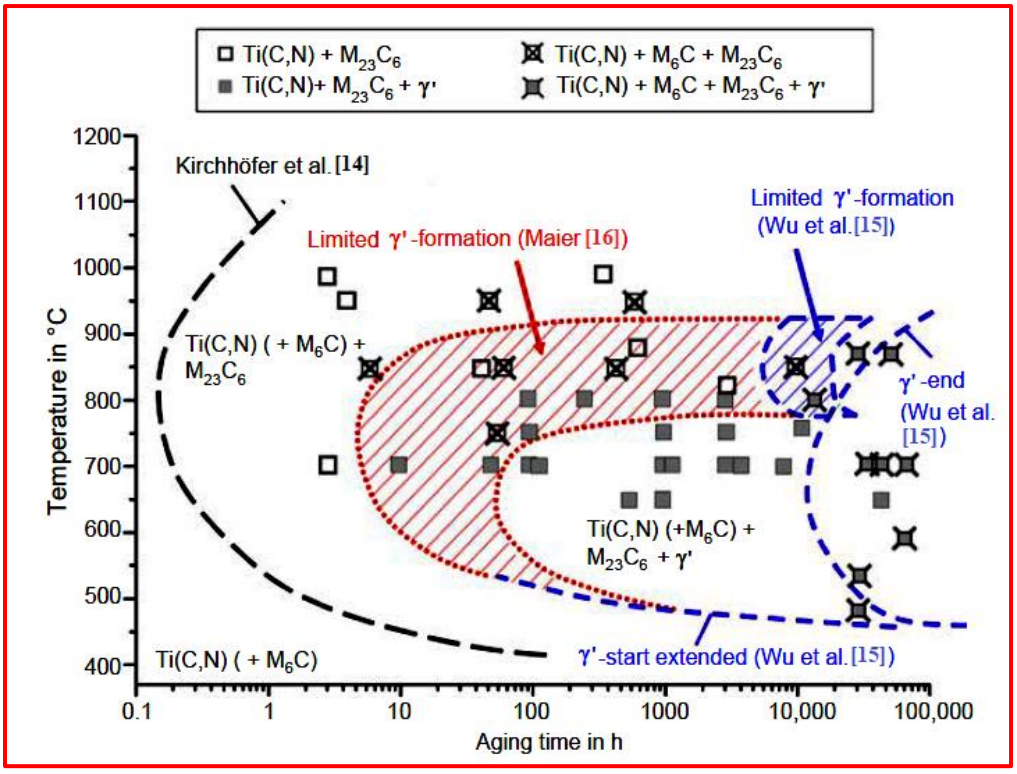

Fig. 1.4: TTT Diagram of Inconel 617 alloy showing temperature and time limits for formation of various phases [3, 14-16].

1.4.3 Applications of Inconel 617 Alloy

Inconel 617, among Ni based super alloys, is the prime candidate material for various high temperature applications due to its excellent creep strength and resistance to oxidation. The following are the critical applications of this alloy [11].

1. Gas turbines of aircraft engines both commercial and military: hot gas path components such as combustor cans, hot gas ducts and transition liners.

2. Advance ultra-supercritical power plants: Tubing of boiler, super heater, re-heater and header pipes.
3. Gas cooled reactors: Tubing of internal heat exchanger (IHX) of the Very High Temperature gas cooled Reactors (VHTR). VHTR is used for the production of hydrogen and electric power generation and is a leading Gen IV advanced reactor in the Next Generation Nuclear Plant (NGNP) program.
4. Chemical processing industries: Catalyst-grid supports in the production of nitric acid
5. Metal processing: Reduction boats in the refining of molybdenum.
6. Heat treatment: Heat-treating baskets.

1.5 Gas Turbine Engines

The gas turbine is an engine that converts chemical energy into mechanical energy. It is an internal combustion engine where the fluid (air) drives the engine and the propeller using the gaseous energy. The gas turbine engine works by four different steps that occur in four different sections. Fig. 1.5 shows all these four sections of the aeroplane gas turbine engine [17]. Fig. 1.6 shows the cross section view with temperature profile at various sections [18].

1. **Inlet section:** This is used for intake of air. Air from atmosphere is drawn and fed into the compressor section.

2. Compression section: The huge amount of air required for combustion and cording of the turbine from hot gases is supplied by the compressor. The compressor draws the air from the atmosphere into the engine via inlet section and compresses it before sending it to the combustion section.

3. Combustion section: In this section, the fuel is injected and is burnt to produce

chemical energy. Combustor is where the fuel and air mix up and burn to release the hot combustor gas to turbine at the required temperature. The combustion section lies in between compressor and turbine section.

4. Turbine and Exhaust Section: Here, the converted energy is put to use. The turbine section of the gas turbine engine has the task of producing usable output shaft power to drive the propeller. In addition, it must also provide the power to drive the compressor and all engine accessories. It does this by expanding the gas at high temperature, pressure, and velocity and converting the gaseous energy to mechanical energy in the form of shaft power. Extra energy is to be added into the system to continue the process, which is provided by the combustor fuel. Chemical energy gets converted to mechanical energy in the turbine section. As the Inconel 617 alloy is mainly used in the components of the hot gas path such as combustor liner and cans in the combustion chambers where high temperatures (up to 1100^{o}C) are predominant, the combustor section is discussed in detail.

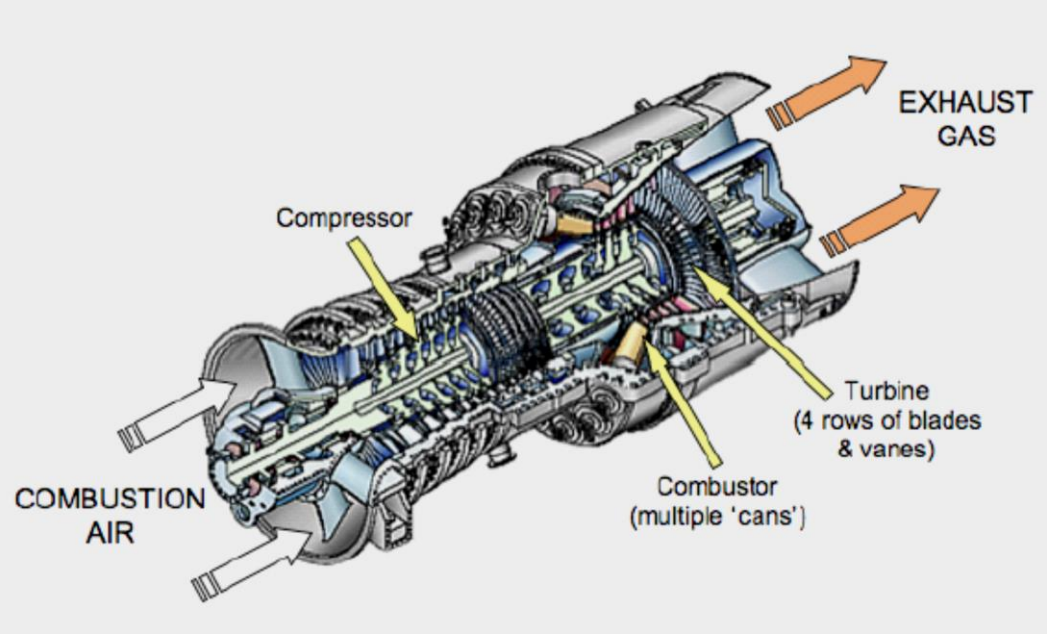

Fig. 1.5: Different sections of the aeroplane gas turbine engine [17].

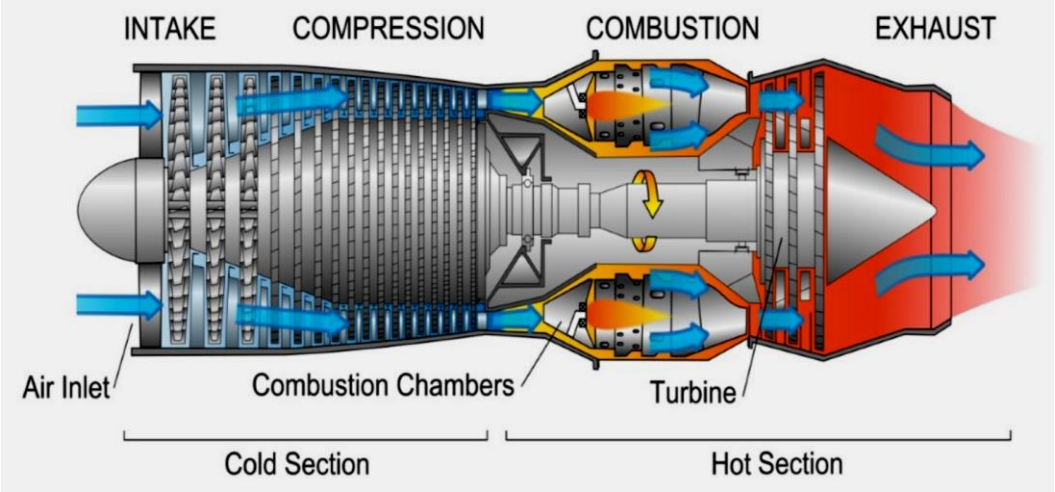

Fig. 1.6: Cross section view of gas turbine engine and temperatures zones of cold and hot section [18].

1.5.1 Combustor Section

Combustion section contains combustion chambers, fuel nozzles, fuel injectors and igniter plugs. Combustion section also contains number of chambers radially arranged around the axis of the engine and the number may vary from 2 to 16. Figs. 1.7 and 1.8 show the details of the combustion chamber [19, 20]. The air for the combustion comes from the compressor and part of it (25% approximately) is consumed for combustion and remaining part (75%) forms as a blanket surrounding the hot gases so that the temperature does not go up and damage the turbine parts. The air used for combustion of fuel is called as primary air whereas the blanket air is called as secondary air. The combustion chamber liners contain holes and or louvers through which the secondary air is passed for cording. The automatic controlled ignition plug ignites the fuel in the starting stage and shuts-off once the process starts. To stop the combustion after the jet engine shuts down, the automatic actuated valves drain out all the excess fuel.

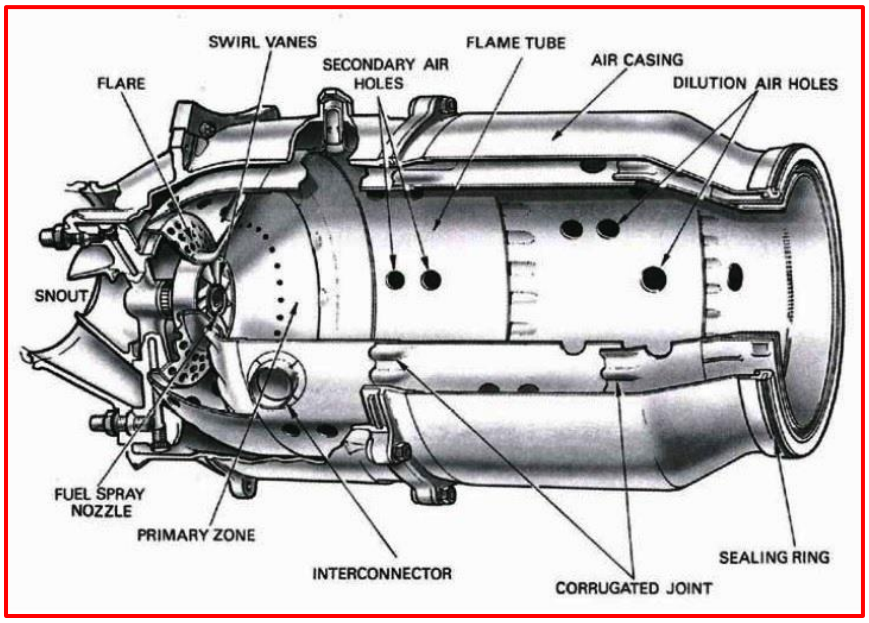

Fig. 1.7: Schematic diagram showing the details of the combustion chamber [19].

The primary functions of the combustion chamber are:

1. Efficient mixing and burning of the air and fuel.
2. Supply of hot gases to the turbine section.
3. Cooling of the hot gases to protect the turbine section especially the blades by cording.
4. Draining the excess fuel after shutdown.

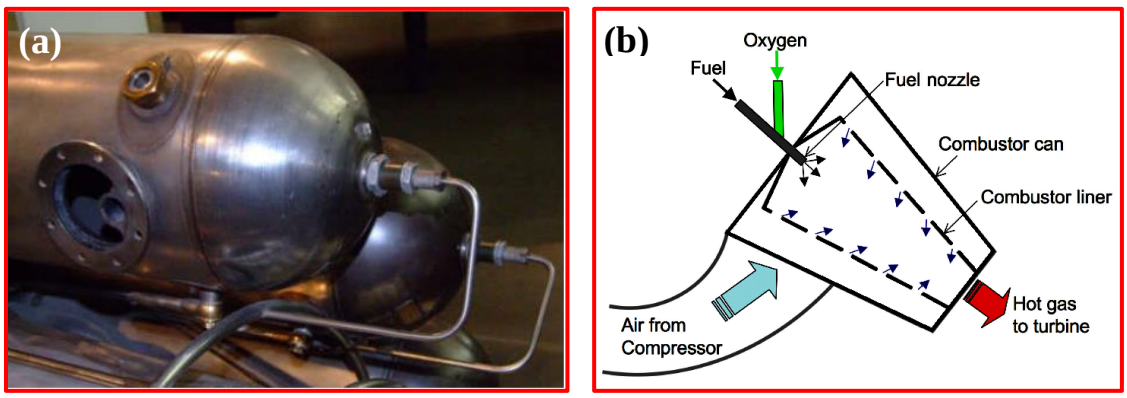

Fig. 1.8: (a) Photograph of the industrial combustion can [20] (b) Schematic showing the principle of the combustion process inside the hot combustion chamber [17].

Performance requirements of the combustion chamber include:

- Efficiency of the combustion should be high with stable operation.
- Combustion must be free from blowout at airflows ranging from idle to maximum power and at pressures representing the aircraft's entire altitude range.
- The pressure losses during flow should be low. High pressure losses will reduce thrust and increase specific fuel consumption.
- Uniform temperature distribution to increase the gas energy and hence the efficiency.
- Quick start up. High pressures and low velocities in the burner make start up easy.
- Combustion section size should be as small as possible, which can accommodate small casings and hence reduce the weight of the engine.
- The burner should release low-smoke as far as possible.
- Low carbon formation: Carbon deposits can block critical air passages and disrupt airflow along the liner walls, causing high metal temperatures and low burner life.

1.5.2 Materials for Combustion Liners

There are mainly three nickel based super alloys available for manufacturing combustion liners namely Inconel 617, Haynes 230 and Hastelloy X [21]. Table1.5 shows the chemical composition of these three alloys. Inconel 617 and Haynes 230 are recent alloys that are developed for successfully replacing Hastelloy X.

The Inconel 617 alloy performs better if the liner is applied with thermal barrier coating (TBC) which provides insulation and reduces the underneath temperature of the base alloy by almost 80^{o}C to 150^{o}C [22]. These coatings also help in mitigating the

uneven temperature distribution effect on the base metal. This is generally done on the hot side of the combustor liner. The TBC of the insulating oxide is applied on the bond coat up to a thickness of approximately 100- 300μm including bond coat. Fig. 1.9 shows the combustion liner which is coated with TBC of yttria stabilized zirconia (YSZ) and micrograph of its cross section showing the thickness of the coating [23, 24]. Detailed introduction and literature review on thermal barrier coatings has been discussed in section 1.11.

Table 1.5: Chemical Composition of Candidate Materials for Combustion Liners in Gas Turbine Engines [21].

Alloy	Cr	Co	Mo	W	Mn	Al	Ti	Si	Fe	C	B	La	Ni
Inconel 617	22.0	12.5	9.0	--	1.0*	1.2	0.6*	1.0*	3.0*	0.1	0.006*	--	Bal
Haynes 230	22.0	5.0*	2.0	14.0	0.5	0.3	--	0.4	3.0*	0.1	0.015	0.02	Bal
Hastelloy X	22.0	1.5	9.0	0.6	1.0*	--	--	1.0*	18.0	0.1	0.008*	--	Bal

* Maximum

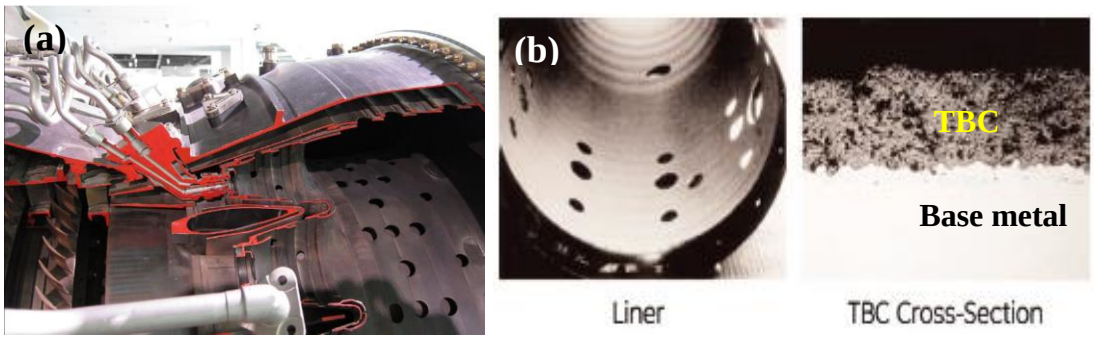

Fig. 1.9: (a) Industrial annular combustor image from Pratt & Whitney JT9D turbine [23] (b) Combustion liner with thermal barrier coating applied on it for improving the performance and details of the coating [24].

1.6 Advanced Ultra Super Critical (AUSC) Power Plants

Coal is considered as the leading source of the power generation for the last two centuries though its importance was decreased after World War II. The usage of

natural gas and oil for the generation of electricity was increased during that period. In 1970s, the crisis of oil forced the world to think about the importance of the coal as the stable energy source. The even distribution of coal reserves placed the coal on top in the list of fuels compared to natural gas and oil and offered an economical solution which contributed for stable growth of coal based thermal power plants. However, for the last three decades (1990-2020), the warnings of global warming due to release of pollutant gases such as CO_2, NO_x, SO_x brought tremendous pressure on the power plants to control the emission of these gases. All over the world, power generation from combustion of fossil fuels is estimated to emit approximately 10 billion tons of CO_2 per year. Similar to the other Asian countries, power generation by coal fired thermal power plants are greatly increased in India to meet the needs of growing population and economy. The continuous pressure to limit the rise in global temperature up to 2^oC gave new challenges to the power plants to look for alternative technologies to reduce the emission of the damaging gases. However, coal being the cheapest source of energy and abundantly available, it remains as prominent fuel. One solution for this, as agreed by renowned global countries, is by increasing the efficiency of the power plant so that for one unit of power generation, the consumption of coal can be reduced.

Conventional power plants are operated with plant efficiencies less than 35% where the steam with temperature around 535^oC and pressure less than 16 MPa are used. Consumption of more coal results in low efficiency and more emission of CO_2. The efficiency of the power plant can be increased significantly by increasing steam parameters such as pressure and temperature. The increase in steam temperature and pressure can be achieved by adapting new technologies for efficient utilisation of the energy. In conventional power plants, water is heated to steam which passes through the steam turbine which in turn drives the power generator. Once the steam passes through

the turbine, it is condensed in condenser and this condensed water again will be reheated in the initial step of the cycle. This is called Rankine cycle. There is loss of heat energy in the final step. Modifications are made to reheat the steam once it is passed through the high pressure turbine instead of condensing, which improves the efficiency of the plant.

Based on the operating parameters, the pulverised coal power plants can be categorised into subcritical, super critical, ultra- supercritical and advanced ultra-supercritical power plants. Table 1.6 gives nomenclature of the various power plants based on efficiency and operating conditions. It can be observed that the efficiency of plants can be increased beyond 45% with AUSC power plant technology [25]. Some other recent technologies have been reported like IGCC (Integrated coal Gasification Combined Cycle) and IGFC (Integrated Gasification Fuel Cell) which are under development stage [26].

Table 1.6: Description of Nomenclature for Various Power Plants [25].

Nomenclature	Steam conditions		Net plant efficiency (%)	CO_2 emissions Kg/MWh
	Pressure	Temperature		
Subcritical	16.5MPa	535 - 550^oC	35	900
Supercritical (SC)	>25MPa	550^oC and above	38	851
Ultra-supercritical (USC)	>25MPa	600^oC and above	>42	836
Advanced ultra-supercritical (A-USC)	28-35MPa	700-760^oC	>45	763

Fig.1.10 shows the increase in plant efficiency with change in steam parameters [27]. It can be observed that increase in temperature of the steam has greater effect on the plant efficiency than the effect by increase in the pressure. Fig.1.11 gives the details of the comparison of CO_2 emissions from 1,000MW coal fired power plants [26]. It is realized that about 12% CO_2 emissions can be reduced by converting USC power plant

to AUSC power plant.

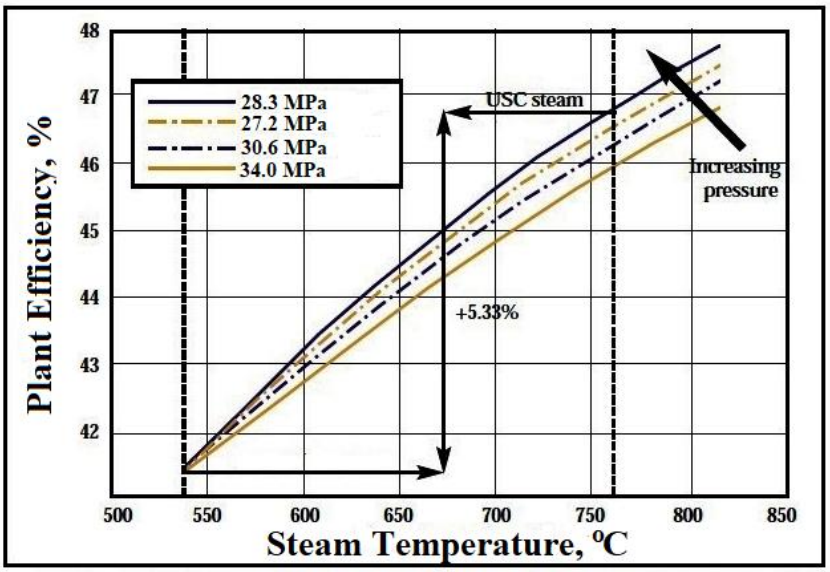

Fig. 1.10: Effect of steam parameters on plant efficiency [27].

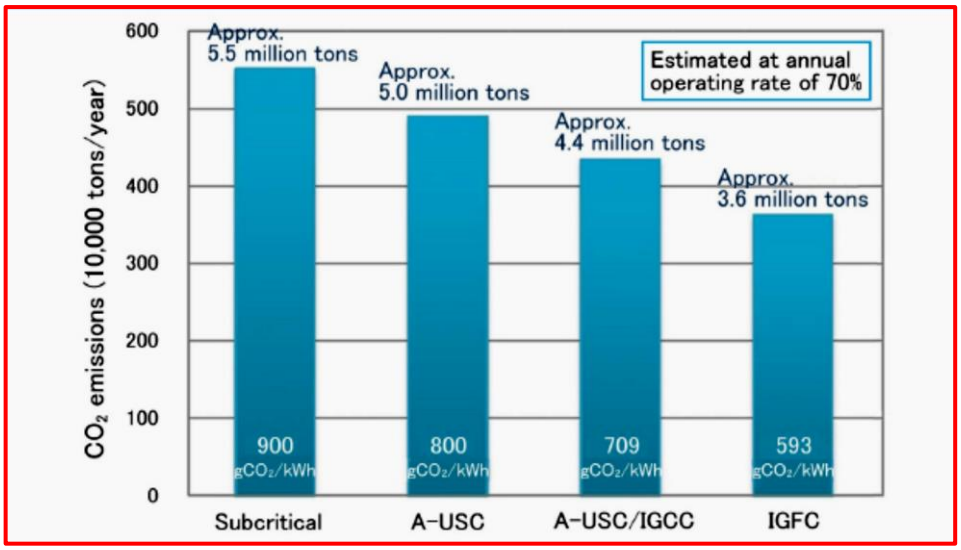

Fig. 1.11: Comparison of CO_2 emissions from 1000MW coal fired power plants [26].

AUSC power plants have a promising technology for increasing efficiency of a thermal power plants and thereby reducing the emissions of CO_2. The final temperature of the steam is generally 100^{o}C more than the steam temperature of the conventional power plants. Fig. 1.12 shows flow diagram of the steam flow in an AUSC power plant. The basic plant layout structure of A-USC power plant is shown in Fig.1.13, which

consists of main boiler, re-heater, primary super heater and secondary super heater as main parts to control the temperature of the steam at various stages.

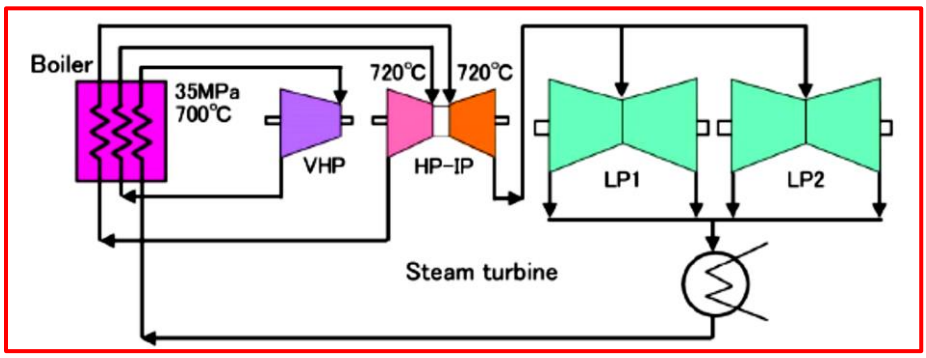

Fig. 1.12: Schematic of the flow of steam in AUSC power plant [26].

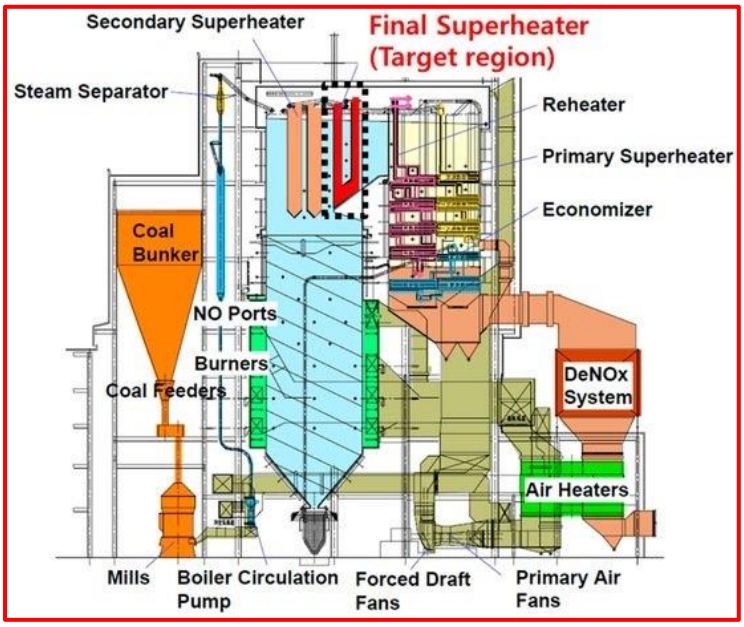

Fig. 1.13: Layout of the AUSC coal fired power plant [26].

1.6.1 Materials for AUSC power plants

The materials used for applications in AUSC power plants should possess the following stringent properties:

- High tensile strength.
- High low cycle fatigue resistance.
- High creep strength.

- Minimum damage from creep–fatigue interaction.
- High structural integrity.
- High workability.
- Good weldability.
- Low co-efficient of thermal expansion
- High thermal conductivity.
- Low cost.

The increase in the steam parameters such as pressure and temperature to increase the efficiency in A-USC power plants necessitates the use of advanced alloys. The requirement of optimum combination of thermal and mechanical properties at those service conditions and also maintaining structural stability at elevated temperatures limit the novel materials available for these applications with due consideration to economics. For subcritical power plants which operate at 550^{o}C and 25MPa, conventional ferritic and martensitic steels can be used. For ultra-supercritical power plants, some of the components subjected to high temperature are replaced or designed with austenitic heat-resistant (A.H.R) steels. For advanced-ultra supercritical power plants where the temperatures are above 700^{o}C and pressures are up to 35MPa, Ni-based superalloys are the best materials to design various components. Fig.1.14 shows the ratio change of high temperature materials with increase in steam parameters used in the development of coal fired power plants [28].

Nickel based superalloys can be used in the main steam pipes, super-heater, re-heater tubes and headers where the steam temperatures are above 700^{o}C. Because these alloys are expensive compared to heat resistant steels, advanced ferritic steels can be used in the major steam piping where the temperatures are below 650^{o}C. Table 1.7 gives details of compositions and specific applications of candidate materials for AUSC

power plants. Inconel 617 superalloy is the prime candidate material for the Advanced Ultra Supercritical (A-USC) power plant applications. Fig. 1.15 shows various materials that constitute the boiler at various sections in AUSC power plants. Creep rupture strength is one of the major properties to be assessed for the material to be used in AUSC power plants.

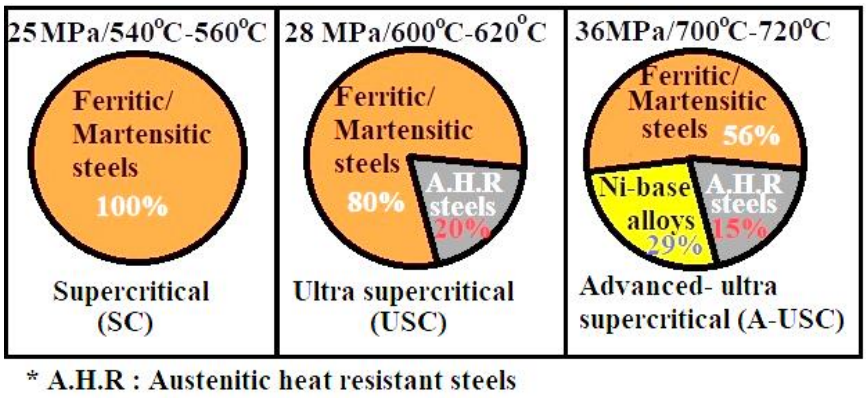

Fig. 1.14: The ratio of change in high temperature materials with steam parameters [28].

Table 1.7: A-USC boiler candidate materials and their applications [26].

Material		**Composition**	**Thick large–diameter pipe**	**Small-diameter tube**
HR6W	Ni-based	45Ni-23Cr-7W	• High temperature header and connecting pipe • Main Steam pipe • Hot reheat steam pipe	Hot heat transfer tube
HR35	Ni-based	50Ni-30Cr-4W-Ti		
Inconel 617	Ni-based	Ni-22Cr-12Co-9Mo-Ti-Al		
Nimonic 263	Ni-based	Ni-20Cr-20Co-6Mo-2Ti-Al	--	
IN740	Ni-based	Ni-25Cr-20Co-2Nb-2Ti-Al		
IN141	Ni-based	Ni-20Cr-10Mo-2Ti-Al		
High B-9Cr steel	Advanced ferritic steel	9Cr-3W-3Co-Nb-V-B	• Header • Connecting pipe (upto ≈650°C)	Heat transfer tube (temperature range similar to conventional high Cr steel)
Low C-9Cr steel	Advanced ferritic steel	0.035C-9Cr-2.4W-1.8Co-Nb-V		
SAVE12AD	Advanced ferritic steel	9Cr-3W-2.6Co-Nb-V-B		

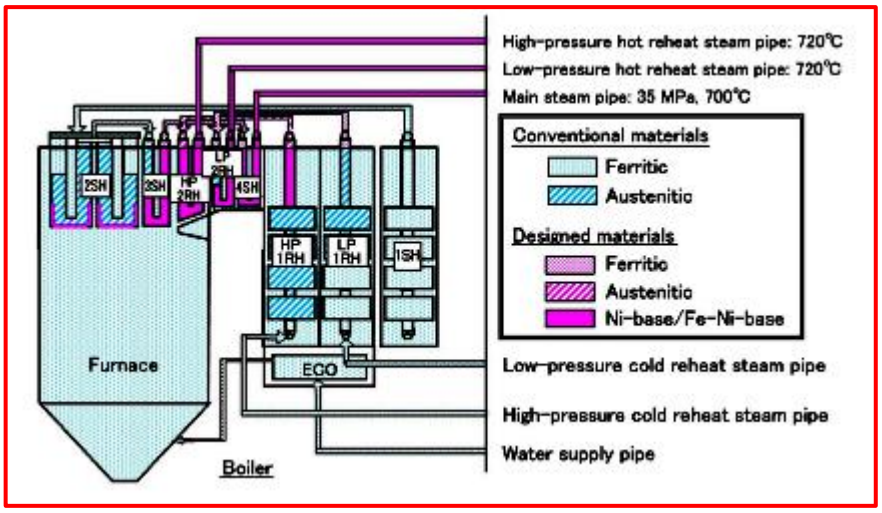

Fig.1.15: Materials used in boilers of AUSC power plants [26].

Fig. 1.16 gives comparison of various materials available in market for usage in AUSC power plants and their comparison of creep rupture strengths [29]. It can be observed from the figure that Inconel 617 withstand temperature of 700 -720^{o}C at minimum desired strength of 100 MPa up to 1,00,000 hours. Inconel 617 alloy along with Haynes 230 are the best solid solution strengthening alloys for this application. Conventional martensitic steels and austenitic steels are placed at lower temperature range than this alloy, whereas age-hardenable alloys such as IN 740, Haynes 282 are placed above the Inconel 617 alloy which can withstand up to 760^{o}C at minimum desired strength.

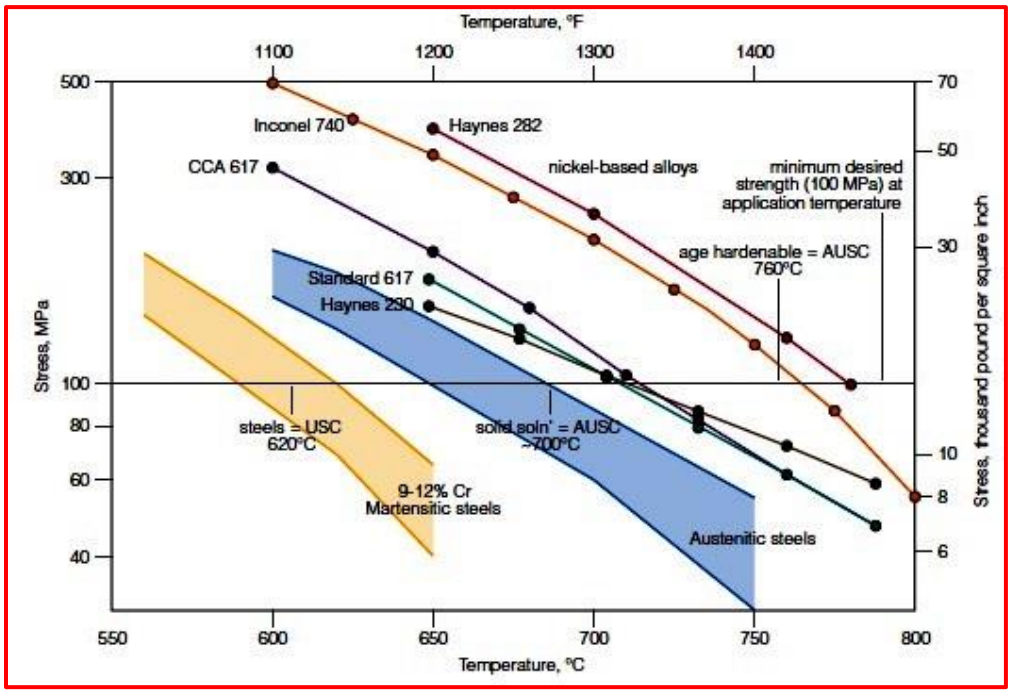

Fig. 1.16: Comparison of various candidate materials available for A-USC power plants [29].

1.7 Dynamic Strain Aging

Investigation of the mechanical properties should be carried out comprehensively for design and safety considerations, because a significant degradation of mechanical properties may occur due to serrated yielding phenomenon in high-temperature environments. Dynamic strain ageing (DSA) is characterized by serrated yielding during plastic deformation. The serrated yielding comes from pinning and unpinning of dislocations by solute interstitials and substitutional atoms, at lower and higher temperatures respectively, also denoted as Portevin–Le Chˆatelier (PLC) effect. This phenomenon results in strain localization under locking conditions (pinning) with sudden increase in applied mechanical stresses. Temperature and strain rate are the two vital factors that influence the occurrence of DSA.

From the literature, the serrations can be categorised in to five forms labelled as type A, type B, type C, type D and type E, based on the appearance of the serrations that

occur due to DSA [30, 31]. Fig. 1.17 shows these five forms of serrations appear in the stress (σ) - strain (ε) curve.

(i) ***Type A***: These serrations are indicated by the sudden rise and drop in the general stress level, and these oscillations are periodic in nature. These are often termed as locking serrations generally occur at high strain rates and at low temperatures in the DSA regime of the alloy.

(ii) ***Type B:*** These are serrations oscillate about the general level of the σ-ε curve and generally preceded by type A. Type B serrations occur in quick succession, unlike type A. These serrations occur at low strain rates and high temperatures.

(iii) ***Type C***: In these serrations the drop in the stress level is below the general level of the σ-ε curve, which occurs due to unpinning of the dislocations. The stress drop level or amplitude is much higher than the A and B type serrations. And these serrations appear at higher temperatures and lower strain rates.

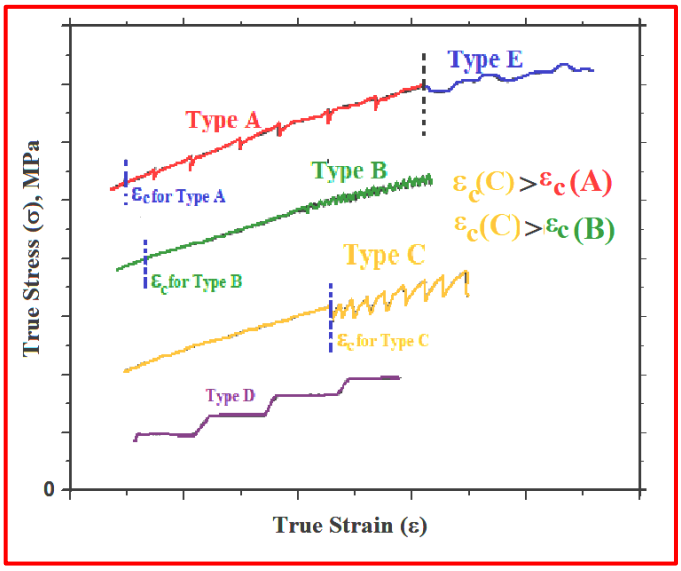

Fig. 1.17: Different types of serrations [31].

(iv) ***Type D:*** These serrations appear as plateaus or steps in the σ-ε curve with no strain hardening or gradient up to certain value of ε. Again the stress level will increase and then maintain the plateau. These type D serrations may occur sometimes in combination with Type B. These type of serrations were reported by Westrum et al. [32] in the case of Au- Cu 14 wt.% alloy.

(v) ***Type E:*** These serrations appear similar to Type A but with small strain hardening, and usually transform from type A serrations at high strain values.

Critical plastic strain (ε_c) for the onset of serrations depends on the strain rate ($\dot{\varepsilon}$) and temperature (T). Fig 1.18 shows the effect of $\dot{\varepsilon}$ and T on ε_c. Increase in temperature decreases the critical plastic strain for the onset of serrations. ε_c increases with increase in strain rate, up to certain strain rate then this relation is vice versa [31].

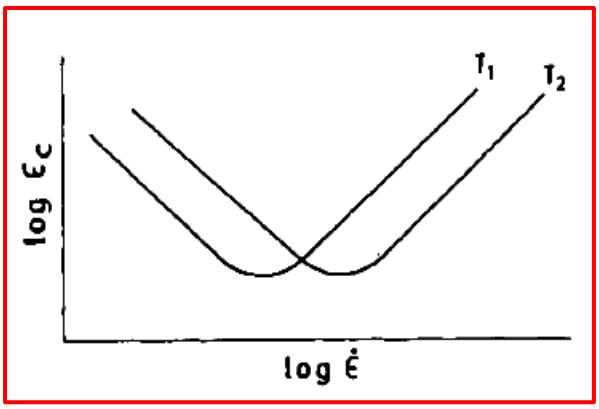

Fig. 1.18: Effect of strain rate and temperature on critical plastic strain, $T_2 > T_1$ [31].

Various manifestations of DSA are shown in Fig. 1.19. With variation in temperature, important features such as plateau in the yield strength, peak in the flow stress, ductility minima, sudden increase or peak in the work hardening rate are seen in the DSA region.

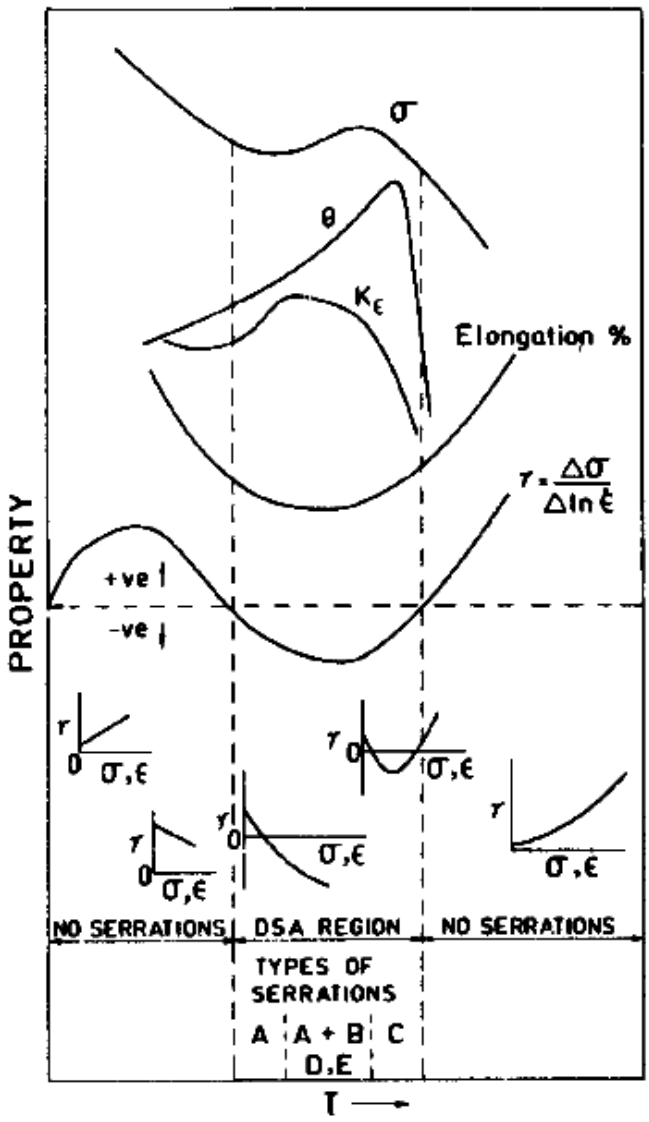

Fig. 1.19: Various manifestations of DSA [31].

DSA has been found to cause deleterious effect on tensile ductility, low cycle fatigue (LCF) life and creep resistance of structural components. Tensile deformation behaviour of the Inconel 617 alloy was studied by several investigators [33-36]. Roy et al. [33] studied the tensile behaviour of the alloy by conducting tensile tests at temperatures ranging from ambient to 1000^{o}C. Fig. 1.20 shows the engineering stress-strain curves obtained indicating serrations in the curves form 200^{o}C to 700^{o}C. Table 1.8 shows the tensile properties reported. Anomalous increase in tensile yield strength (YS) of Inconel 617 alloy at 800°C and 900°C was observed. The enhancement in YS

was attributed to the formation and accumulation of $Cr_{23}C_6$ and $Mo_{23}C_6$ precipitates, and development of pinned dislocations, dislocation pile-ups, and subgrains in the vicinity of the grain boundaries. The reduced ductility in terms of failure strain at 100°C was the result of DSA.

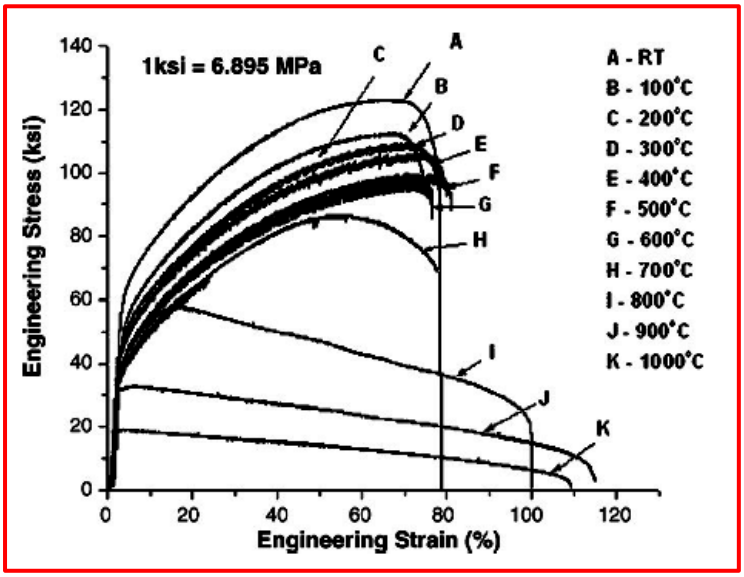

Fig. 1.20: Engineering stress- strain curves of Inconel 617 alloy from RT to 1000°C. Serrations were observed from 200°C to 700°C [33].

Table 1.8: Tensile Properties of Inconel 617 Alloy at Various Temperatures [33].

Temperature, °C	YS, MPa	UTS, MPa	% Elongation	% RA
30	371	856	78.35	61.98
100	306	774	74.40	56.88
200	283	761	78.41	60.17
300	265	752	77.71	56.20
400	254	728	79.90	57.41
500	244	697	78.68	53.74
600	221	688	79.05	48.56
700	211	598	80.83	48.44
800	234	392	100.23	73.02
900	237	240	84.49	78.53
1000	131	131	88.23	72.07

Kauomi et al. [34] have studied deformation mechanism of this alloy at high temperatures. Tensile tests at 25°C, 600°C, 800°C and 950°C were conducted in air at strain rates ranging from 10^{-5} to 10^{-3} s^{-1} to study the temperature and strain rate effect on the tensile properties of Inconel 617 alloy in comparison to those of Haynes 230. Above 300°C, strain hardening was accompanied by saw-tooth type serrations with amplitudes ranging from 10 to 25 MPa. Sinusoidal serrations were observed with softening at the highest temperatures and were smaller in amplitude, about 2–5 MPa. The saw-tooth type serrations observed with hardening at intermediate temperatures (300–800°C) were associated with dynamic strain aging. Variation in types of serrations with respect to temperature is shown in Fig. 1.21**.** The YS decreased up to 600°C, followed by an increase up to 850°C which was termed as yield strength anomaly, and then decreased at 900°C and above.

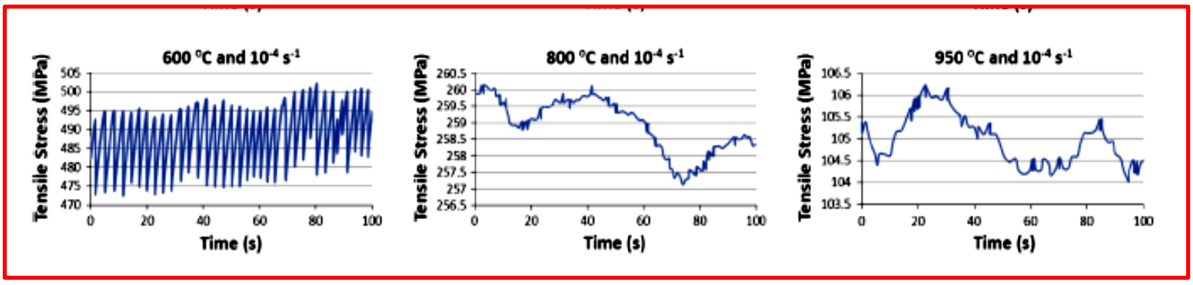

Fig. 1.21: Variation in serrations with change in temperature [34].

Wright et al. [35, 36] characterized the variation of elevated temperature properties of Inconel 617 alloy with respect to temperature and strain rate. Tests were conducted at RT and from 650°C to 1000°C at 50°C intervals. They confirmed DSA region from 600°C to 850°C. Fig. 1.22 shows stress strain curves obtained in the study with occurrence of serrations up to 750°C.

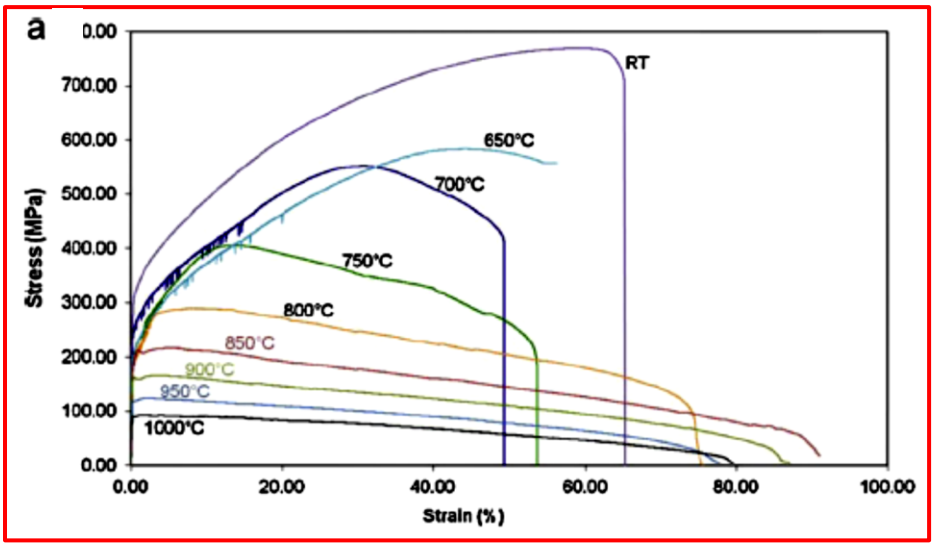

Fig. 1.22: Stress strain curves of Inconel 617 alloy [35].

Mo et al. [37] studied deformation mechanism of Inconel 617 alloy by conducting tensile tests up to 1000^{o}C and reported occurrence of DSA based on serrated flow. They also studied strain rate sensitivity of the alloy [38]. The effect of orientation of grains was studied in detail by Mo et al. [39] using tensile testing of specimens taken at various angles to the rolling direction. Loss of transverse strength was observed compared to the strength in the longitudinal direction.

Ekaputra et al. [40] reported DSA in Inconel 617 alloy, however, attention was not paid to understand the controlling mechanisms of DSA, various manifestations of DSA, characterization of deformation behaviour and fracture behaviour. High-temperature tensile tests were carried out with variations in strain rate of 10^{-3} s^{-1}, 10^{-4} s^{-1} and 10^{-5} s^{-1} from 24^{o}C to 950^{o}C. Five flow relationships namely, Hollomon, Ludwik, Swift, Ludwigson, and Voce relationships [41-45] were applied to describe the tensile true stress-true plastic strain curves, and the DSA region was defined. Fig. 1.23 shows true stress- true plastic strain curves with concave upward curve which indicate deviation from Hollomon relationship and fitted with various flow relationships.

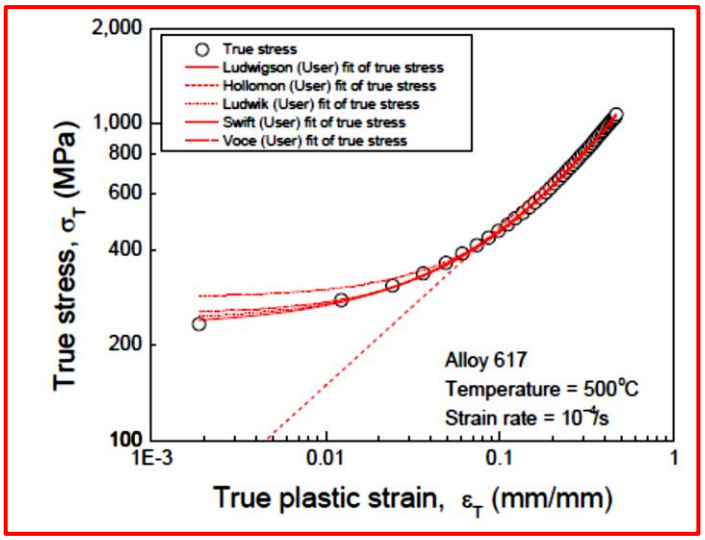

Fig. 1.23: Flow relationships for tensile samples of Inconel 617 alloy tested at 500°C and at a strain rate of 10^{-4} s^{-1} [40].

1.8 Effect of Heat treatment and Thermo-Mechanical Treatment on Tensile Deformation Behaviour

Several researchers have studied Inconel 617 alloy in solution annealed condition [12, 13, 46, 47]. Hosier and Tillak [13] initially studied its creep rupture strength, resistance to oxidation and corrosion in the solution annealed condition, at elevated temperatures (980°C-1150°C). They found the properties to be superior to those of the Inconel 625 at higher temperatures, in all respects. Mankins et al. [12] studied the effects of long-time exposure at temperatures up to 1093°C under stress, on microstructure and phase stability of Inconel 617 alloy. They found precipitation of $M_{23}C_6$ carbide as prime means of its strength at elevated temperature. Kirchoffer et al. [14] varied aging time and temperature following solution annealing to study evolution of carbides and their effect on hardness and observed increase in hardness with increase in aging time. Kimball et al. [48] examined changes in microstructure and mechanical properties of Inconel 617 alloy during aging at temperatures in the range 593 to 816°C for exposures up to 8000 h and observed age hardening at all the temperatures except at 760°C where softening was observed for long durations of aging. Aging behaviour of

the alloy at 900^{o}C and 1000^{o}C up to 3000 hours was studied by Mo et al. [49]. They reported increase in mechanical properties in the initial stages of aging and softening due to prolonged aging. Wu et al. [15, 50] studied the effect of long-term aging (up to 65,000 h) on microstructure of Inconel 617 alloy and confirmed that $Cr_{23}C_6$, Mo-rich η-M_6C, and Ti (C, N) constitute the major coarse precipitates both within the grains and along the grain boundaries. Also Liu et al. [51] investigated the effect of thermal aging on mechanical properties of this alloy and found that there was reduction in yield strength and ultimate tensile strength after aging for 10000 h due to coarsening of $M_{23}C_6$ precipitates. Jo et al. [52] studied the effect of long exposure of up to 1000 h at 1050^{o}C and found formation of protective Cr oxide layer, coarsening of carbides and marginal change in mechanical properties. Several researchers studied the effect of heat treatment and initial microstructure on creep properties of Inconel 617 alloy [53-55]. Chomette et al. [53] studied creep behaviour of this alloy in solution annealed, aged at 850^{o}C and 950^{o}C, and 20% cold worked condition. They observed grain boundary migration and recrystallization at 850^{o}C. Sharma et al. [54] studied effect of rolling and annealing of Inconel 617 alloy foils on its creep properties at 900^{o}C and 35MPa. Recrystallization and grain growth was observed in cold rolled specimens on annealing at 950 and 1100^{o}C. Effect of cold working on creep rupture properties of this alloy was extensively studied by Wright et al. [55]. At 900^{o}C, creep rate, strain to failure and time to rupture were significantly reduced in the cold worked material with respect to those of the solution annealed material. Effect of long term aging at 750^{o}C for 1,000 to 20,000h was studied on work hardening behaviour of Inconel 617 at room temperature by Singh et al. [56]. Increase in the rate of work hardening was observed and was attributed to precipitation of γ′ [Ni_3(Ti,Al)].

1.9 Low Cycle Fatigue Behaviour of Inconel 617 Alloy

Structural components which are operated at high temperatures experience thermal stresses because of the difference in temperature from the outer surface to the inner core of the component. These thermal stresses may exceed the yield stress of the material and cause low cycle fatigue (LCF) damage in the material. LCF damage also occurs due to the start–up and shutdown operation cycles of the component. In case of transient conditions, increase in thermal stresses and temperatures become much higher than that of the normal operating conditions. Fig. 1.24 shows temperature profiles during start up and shut-down of the gas turbine engine.

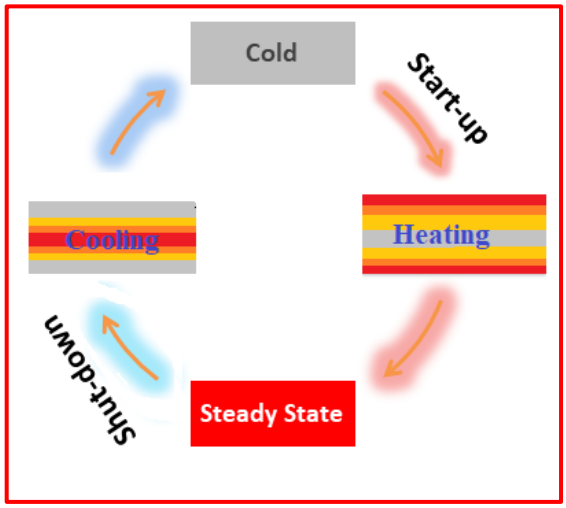

Fig. 1.24: Temperature profiles during start up and shut-down of the gas turbine engine.

At high temperatures, fatigue damage and life are influenced by several time–dependent mechanisms such as dynamic strain ageing (DSA), oxidation, corrosion, creep and stress induced precipitation that occur concurrently with cyclic loading. These damage processes are strong functions of temperature and environment. The occurrence of DSA, which involves interaction of solutes with mobile dislocations during high temperature low cycle fatigue in certain range of temperature and strain rate, leads to reduction in strain controlled fatigue life [57]. Environment such as salt coating and

thermal barrier coating also influence the fatigue life of the components. Application of Inconel 617 alloy in air craft based gas turbine applications where the air intake contains salts at elevated temperatures, exposes it to deleterious salt environment and causes severe hot corrosion. The fused salt deposits of Na_2SO_4 and NaCl attack the surface of the material at high temperature and accelerate the corrosion processes [58]. NaCl is mainly accrued from the combustion air of the environment in the form of tiny particles and its reaction with sulphur from fuel forms Na_2SO_4. In addition, the material also experiences thermal stresses and localised plastic strains due to high temperatures during repeated start up and shut down events of the gas turbine engine. Consideration of LCF data under oxidising and saline environment is therefore of utmost importance while designing components of gas turbine engines and thus forms the basis of the present investigation. Thermal barrier coating on the components reduce the temperature of the base metal that is exposed to the hot gases in the combustion chamber. These coatings can change the deformation behaviour as well as the fracture behaviour under cyclic loading. However, studies on the effect of salt coating as well as thermal barrier coating on low cycle fatigue behaviour along with deformation and fracture behaviour of superalloys in general and Inconel 617 alloy in particular are limited.

Rao et al. [57] conducted strain controlled low cycle fatigue tests on Inconel 617 alloy in air to ascertain the influence of strain rate ($\dot{\varepsilon}$ ranging from $4x10^{-6}$ s^{-l} to $4x10^{-3}$ s^{-l}) and temperature (T ranging from 750/850/950^{o}C) and reported decrease in the number of cycles for initiation of macro crack with decrease in strain rate and increase in temperature. A reduction in fatigue life was observed with decreasing strain rate ($\dot{\varepsilon}$) at 850^{o}C and with increasing temperature at strain rate ($\dot{\varepsilon}$) of $4x10^{-5}$ s^{-1}. Table 1.9 shows the effect of strain rate and temperature on low cycle fatigue properties. Hysteresis

loops at 850°C exhibited serrations in the loops which is an indication of DSA (Fig. 1.25). Strengthening of the matrix due to dynamic strain aging of matrix by dislocations and by precipitation of $M_{23}C_6$ carbides led to brittle fracture of grain boundary carbide films formed at 750°C and crack propagation was intergranular.

Strizak et al. [59] studied the effect of environment on LCF properties of Inconel 617 alloy in solution annealed and aged conditions at 538°C, 704°C and 871°C and reported little or no change in its fatigue resistance in impure helium in comparison to that in air. Strain-controlled fully reversed fatigue tests were conducted at a cyclic strain rate of $4x10^{-3}$ s^{-1}. Fatigue tests were conducted in air and in a typical service environment for gas-cooled reactors, which is impure helium. The composition of the gas was 30.39 Pa (300 μ atm) H_2, 3.04 Pa (30 μ atm) CH_4, 2.02 Pa (20 μ atm) CO, and 0.20 Pa (2 μ atm) H_2O, and the gas pressure in the environmental chamber was 83 kPa (1.8 atm). Comparison of fatigue behaviour of various materials at 538°C is shown in Fig. 1.26 [59].

Table 1.9: Effect of Temperature and Strain Rate on Low Cycle Fatigue Properties [57].

Sample Code	T (°C)	$\Delta\varepsilon$ (Pct)	$\dot{\varepsilon}$ (s^{-1})	N_A (Cycles)	N_F (Cycles)	$(\sigma_T)_{1/4}$ (MPa)	$(\sigma_T)_{NA/2}$ (MPa)	Serrated Flow (Cycles)	
								Tension	Compression
AUW2	850	0.6	4×10^{-3}	745	882	205.6	227.3	¼ to 850	1 to 790
AUW4	850	0.6	4×10^{-3}	798	1014	204.7	284.6	¼ to 950	1 to 870
AUW8	850	0.6	4×10^{-3}	889	1151	203.8	286.0	¼ to 1000	1 to 1000
AUW10	850	0.6	4×10^{-3}	754	886	205.6	285.7	¼ to 970	1 to 1030
AUW3	850	0.6	4×10^{-4}	598	763	207.5	249.3	1 to 5	1 to 650
AUW6	850	0.6	4×10^{-4}	660	814	208.3	246.1	1 to 5	1 to 720
AUW11	850	0.6	4×10^{-4}	703	886	209.2	250.2	1 to 81	1 to 720
AUW5	850	0.6	4×10^{-5}	612	845	205.0	168.5	—	—
AUW7	850	0.6	4×10^{-5}	554	674	202.9	167.8	—	—
AUW9	850	0.6	4×10^{-5}	556	710	205.0	169.0	—	—
AUW14	850	0.6	4×10^{-5}	577	744	206.7	167.5	—	—
AUW18	850	0.6	4×10^{-6}	426	534	131.0	111.8	—	—
AUW20	850	0.6	4×10^{-6}	477	594	129.8	111.3	—	—
AUW15	950	0.6	4×10^{-5}	512	604	113.0	94.5	—	—
AUW16	750	0.6	4×10^{-5}	628	702	212.1	323.6	2 to 11	1 to 610

$(\sigma_T)_{1/4}$ = tensile stress amplitude in the first quarter cycle.
$(\sigma_T)_{NA/2}$ = tensile stress amplitude at half of the life for macrocrack initiation.

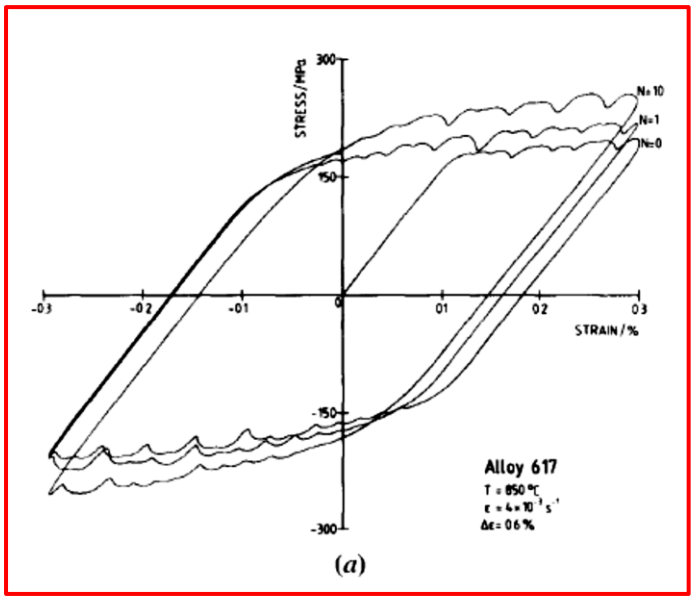

Fig. 1.25: Serrations observed in hysteresis loops for the samples fatigue tested at 850°C at strain amplitude of ± 0.6% [57].

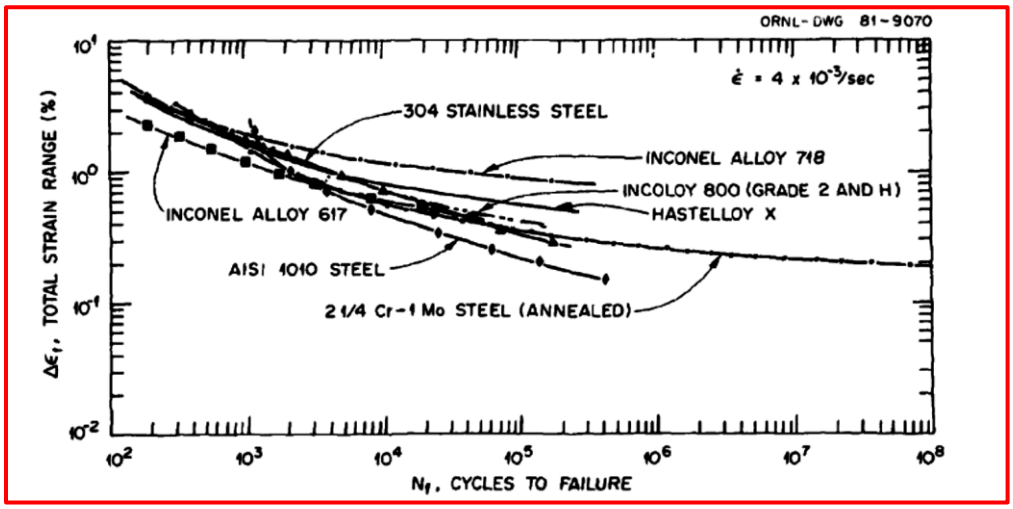

Fig. 1.26: Comparison of fatigue behaviour of several materials at 538°C [59].

Wright et al. [60] reported deformation by plastic flow at 850°C and solute drag creep in alloy Inconel at 950°C during LCF loading. Fig. 1.27 Coffin-Manson plot for LCF tests at 10^{-3} s^{-1}, showing slope of approximately -1.0 when inelastic strain is plotted as a function of fatigue life.

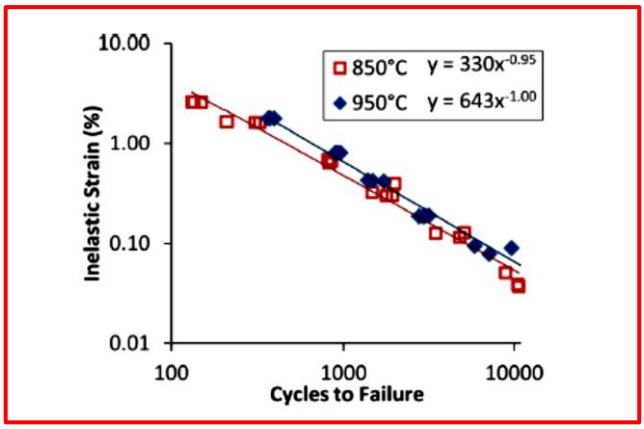

Fig. 1.27: Coffin-Manson plot for LCF behaviour of Inconel 617 at 10^{-3} s^{-1} [60].

Burke and Beck [61] performed LCF tests at 760°C and 871°C and observed intragranular slip (sliding) stabilized by fine carbide particle precipitation and grain boundary sliding as primary mechanisms of deformation at these temperatures respectively. Srivastava and Klarstrom [62] performed LCF tests on Inconel 617 alloy at 760°C, 871°C and 982°C to compare with the LCF behaviour of Haynes 230 alloy and Haynes alloy X and showed that oxidation played a key role in fatigue crack initiation. LCF behaviour of Inconel 617 alloy at room temperature, 760°C and 871°C was also studied by Smith and Yates [63]. It was confirmed that the grain size in the range of ASTM 4 to 5 was good for LCF life and elevated temperature properties. Shankar et al. [64] confirmed the occurrence of dynamic strain aging in alloy 617M under strain controlled cyclic loading. Stress response curves obtained for the samples tested at 500°C in the study are shown in Fig. 1.28a which reveal cycling hardening. Rate of hardening with respect to fatigue life (%) is shown in Fig 1.28b**.** Fig.1.29 shows precipitates at 750°C as well as sub grain boundaries and precipitates at 850°C.

However, only limited investigations have been carried out on the comparative evaluation of fatigue properties, deformation and fracture behaviour of Inconel 617 at room temperature and 750°C. The deformation behaviour of Inconel 617 alloy subjected

to cyclic loading at room temperature and 750°C by detailed transmission electron microscopy and diffraction analysis has also not been reported, though many studies on deformation behaviour above 850°C are published.

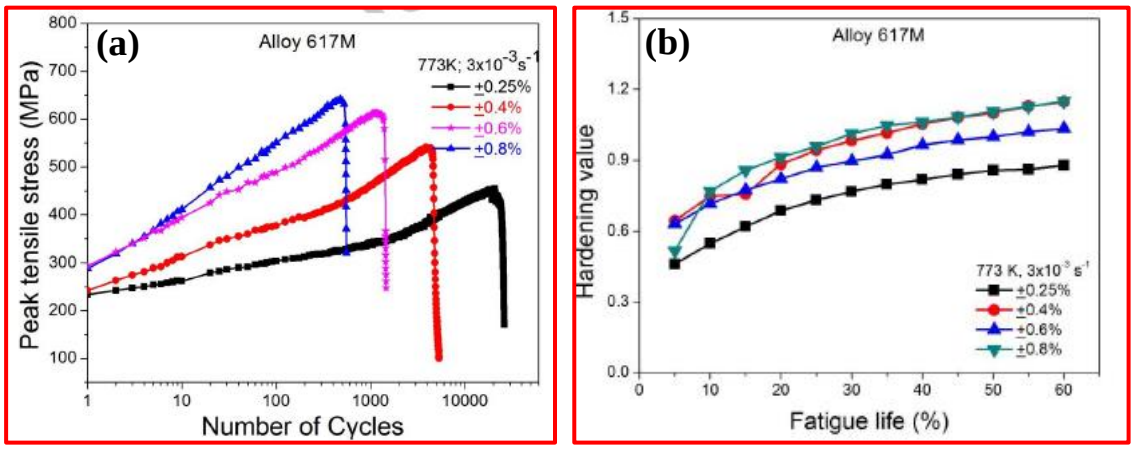

Fig. 1.28: (a) Cyclic stress response curves of Alloy 617M alloy fatigue tested at 500°C (b) rate of hardening with respect to fatigue life [64].

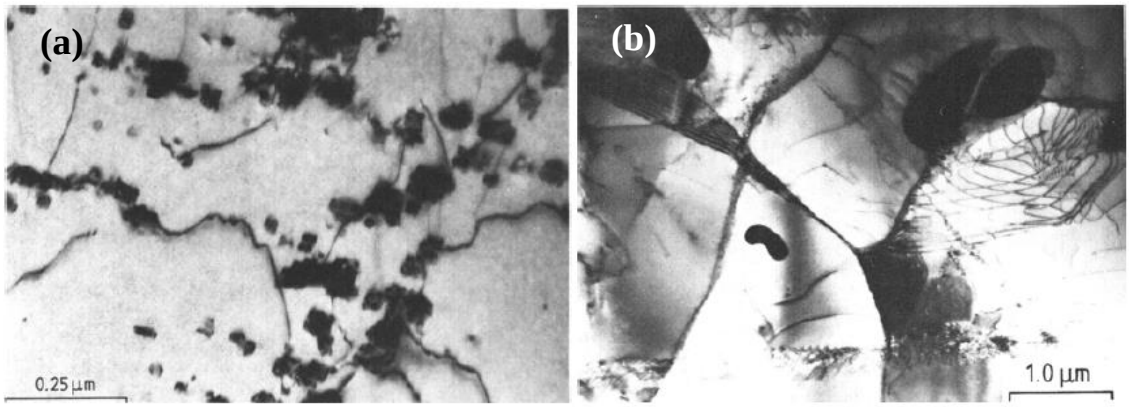

Fig. 1.29: TEM micrographs of fatigue tested samples, showing (a) precipitates at 750°C (b) sub grain boundaries and precipitates at 850°C [57].

1.10 Effect of Hot Corrosion on Low Cycle Fatigue Behaviour

1.10.1 Hot Corrosion

In general, metals and alloys experience accelerated oxidation when their surfaces are covered with a thin film of fused salt in an oxidizing atmosphere at elevated

temperatures. This is known as high temperature or 'hot' corrosion where a porous and non-protective oxide scale is formed on the surfaces along with sulphides in the substrate and it does not involve aqueous electrolytes. Hot corrosion is basically the result of attack by fuel and/or ash compounds of Na, V, S, and Cl that are present in the coal or in fuel oil used for combustion during applications. In some situations, these impurities may be ingested from the service environment. For instance, NaCl contamination is mainly from marine atmospheres. There is a general agreement that condensed alkali metal salts including (notably) Na_2SO_4, are prerequisite to hot corrosion [65]. Apart from Na_2SO_4, V_2O_5 also causes high-temperature corrosion in these applications. Due to high cost of removing these impurities, the use of the low grade fuels is usually justified. Sodium vanadyl vanadate ($Na_2O.V_2O_4.5V_2O_5$), which melts at relatively low temperature of 550°C, is found to be the most common salt deposit on boiler super heaters [66]. Similarly, the predominant compounds in the salt deposits on gas turbine surfaces are reported to be Na_2SO_4, V_2O_5, and $Na_2V_2O_6$ [67].

Due to the depletion of high-grade fuels and for economic reasons, use of residual fuel oil in the energy generation equipment is well known. Residual fuel oil contains sodium, vanadium, and sulphur as impurities, as well as salts such as NaCl due to contamination from entrained brine. Sodium and sulphur form Na_2SO_4 (melting point 884°C) by reaction in the combustion system. The Na_2SO_4 can be ingested in the turbine intake air or it can be produced by a reaction between sodium chloride (NaCl) ingested with the intake air and sulfur impurities in the fuel [58]. During combustion of the fuel, vanadium reacts with oxygen to form an oxide, V_2O_5 (melting point 670°C). Thus V_2O_5 is in liquid state at gas turbine operating temperatures. These compounds known as ash, deposit on the surface of the alloys used in power generation equipment and induce accelerated oxidation (hot corrosion).

1.10.2 Effect of Hot corrosion on Low Cycle Fatigue Behaviour

Several researchers have studied the oxidation and hot corrosion behaviour of Inconel 617 alloy under static conditions [68-71]. Khan et al. [68] have studied hot corrosion behaviour of Inconel 617 alloy at 900°C and 1000°C under static conditions in salt environment of NaCl, Na_2SO_4 and V_2O_5. They found that rate of oxidation was insignificant compared with that of mixed salt environment. $NiCr_2O_4$ and $NiMoO_4$ spinel oxides contributed to corrosion resistance. El-Awadi et al. [69] compared the behaviour of superalloys Inconel 617 and IN 738 by studying static hot corrosion at 700°C, 800°C and 900°C for different durations, up to 100 hours, under mixed salt environment of NaCl and Na_2SO_4. Fig. 1.30a shows weight change/surface area (mg/cm^2) versus time plot for Inconel 617 alloy subjected to hot corrosion for 100h at 700°C, 800°C and 900°C. Fig. 1.30b shows the values of parabolic rate constant

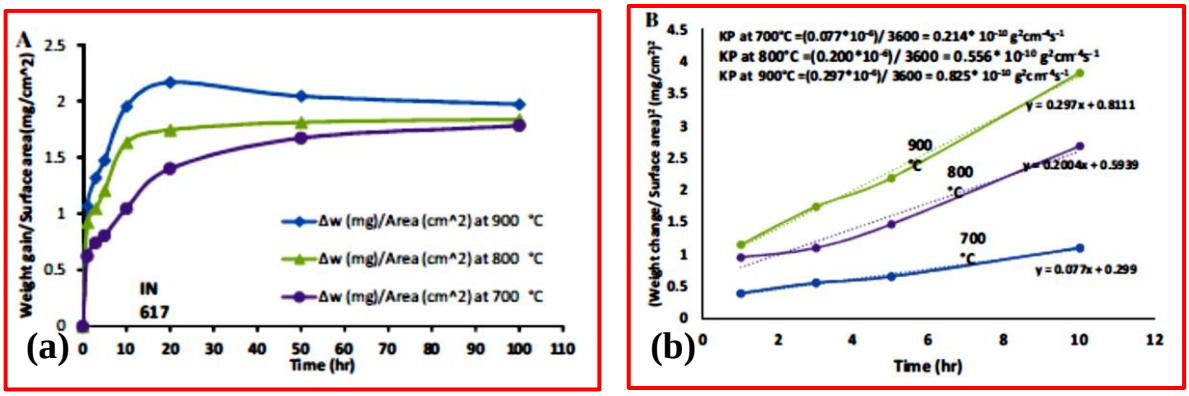

Fig. 1.30: Weight change/ surface area (mg/cm^2) versus time plot for Inconel 617 subjected to hot corrosion for 100h at 700°C, 800°C and 900°C (b) The parabolic rate constant on the basis of the first 10h exposure time, for Inconel 617 [69].

obtained on the basis of the exposure time for first 10 hours, for Inconel 617. Fig. 1.31 shows XRD patterns of Inconel 617 alloy after hot corrosion at 800°C and at 900°C. They found that $NiCr_2O_4$ and $CoCr_2O_4$ spinels along with Cr_2O_3 provided corrosion resistance to these alloys.

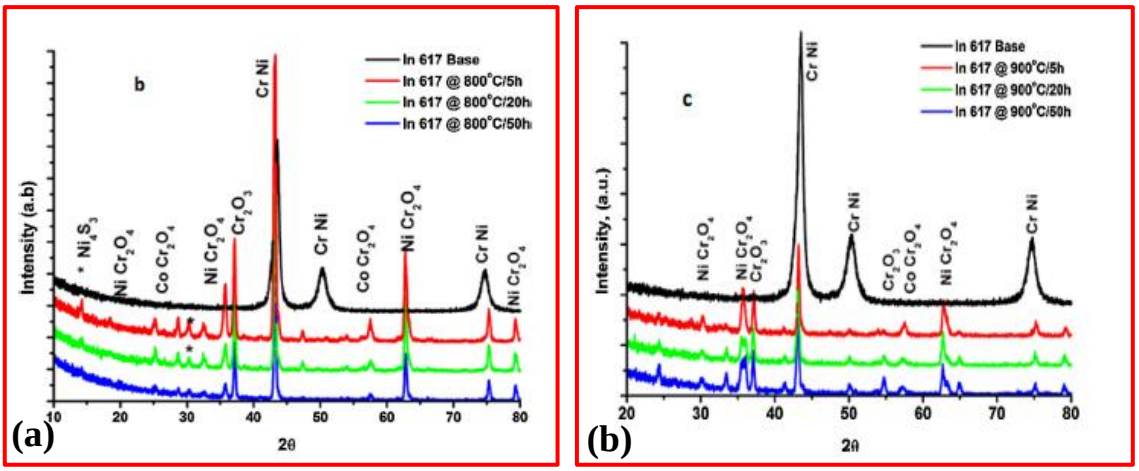

Fig. 1.31: XRD pattern of Inconel 617 alloy after hot corrosion at (a) 800°C and (b) at 900°C [69].

Fig. 1.32 shows cross sectional images of Inconel 617 alloy samples oxidised in air at 850°C and 950°C up to 12 cycles and EDX elemental analysis maps at 950°C. Eliaz et al. [70] have reviewed different case studies of blades of gas turbine subjected to hot corrosion. They categorised hot corrosion processes into Low Temperature Hot Corrosion (LTHC) and High Temperature Hot corrosion (HTHC). LTHC generally occurs in the temperature range from 650-800°C whereas HTHC occurs in the temperature range from 800-950°C [70, 71]. Pettit et al. [72] reviewed in detail the studies on hot corrosion behaviour of various superalloys under mixed salt environments. Various mechanisms of hot corrosion were summarised in detail and formation of porous oxide scales and sulphides in the base metal were identified as the main cause of failures. Fig. 1.33a and b show optical micrographs revealing corrosion of Inconel 617 after exposure for 100h and 4ppm Na_2SO_4 at 900°C, attack at grain boundaries causing the detachment of grains beneath the scale and internal corrosion and grain boundary attack 1000°C.

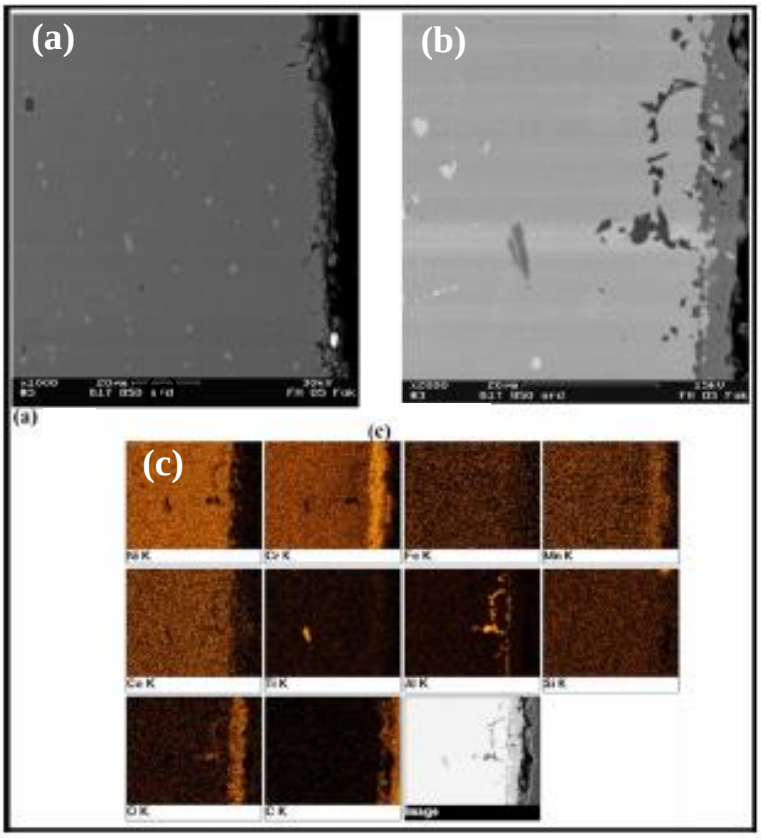

Fig. 1.32: Cross sectional images of alloy Inconel 617 samples oxidised in air for 12 cycles: (a) at 850^{o}C (b) at 950^{o}C and (c) EDX elemental analysis map at 950^{o}C [69].

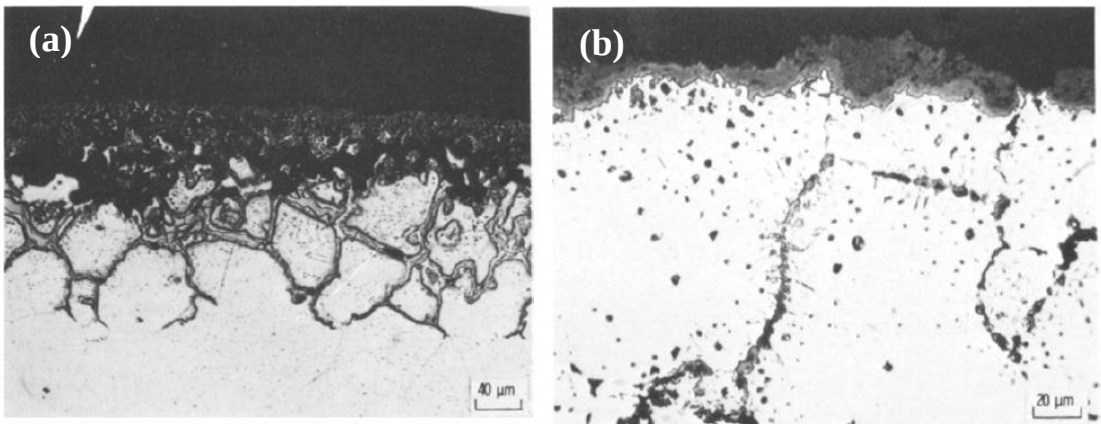

Fig. 1.33: Optical micrographs showing corrosion of IN 617 alloy exposed for 100hr and 4ppm Na_2SO_4: (a) at 900^{o}C and (b) at 1000^{o}C [72].

Several researchers have conducted LCF tests under salt environment to study its influence on fatigue behaviour of various superalloys [73-76]. Yang et al. [73] studied influence of hot corrosion (75%Na_2SO_4+25%NaCl) on LCF behaviour of

DZ125 nickel based superalloy at 850^{o}C and observed reduction in fatigue life in salt coated samples due to early premature failure from the weak grain boundaries because of intergranular corrosion. Jianting et al. [74] studied LCF behaviour of the IN738LC alloy at 900^{o}C, under vacuum, air and salt (75%Na_2SO_4+25%NaCl) environments. They found that cracks initiated always at corroded grain boundaries near the surface and crack propagation was transgranular. Sahu et al. [75] have studied the influence of hot corrosion (10% NaCl + 90% Na_2SO_4) on LCF behaviour of SU263 at 800^{o}C and observed reduction in fatigue life for the samples with salt coating, for samples tested at same strain amplitudes compared to the life of tested sample without coating. Mahobia et al. [58, 76] have conducted extensive studies on the effect of saline environment on low cycle fatigue life of GTM-SU-718 at 550^{o}C and 650^{o}C and found drastic reduction in fatigue life with increase in pre exposed duration after salt coating. Table 1.10 shows the fatigue data for the same. Fig. 1.34 shows cyclic stress response curves for the superalloy GTM-SU-718 at room temperature.

Table 1.10: LCF data at Room Temperature for the Alloy GTM-SU-718 [76].

Condition	Exposure time and temperature	Cycles to failure (N_f)
Uncoated	No exposure	1002
Uncoated	25hrs at 550^{o}C	1119
Uncoated	25hrs at 650^{o}C	1132
3.5 wt.% NaCl	25hrs at 550^{o}C	651
75 wt.% Na_2SO_4 + 25 wt.% NaCl	25hrs at 650^{o}C	1594
90 wt.% Na_2SO_4 + 5 wt.% NaCl + 5 wt.% V_2O_5	25hrs at 650^{o}C	1136

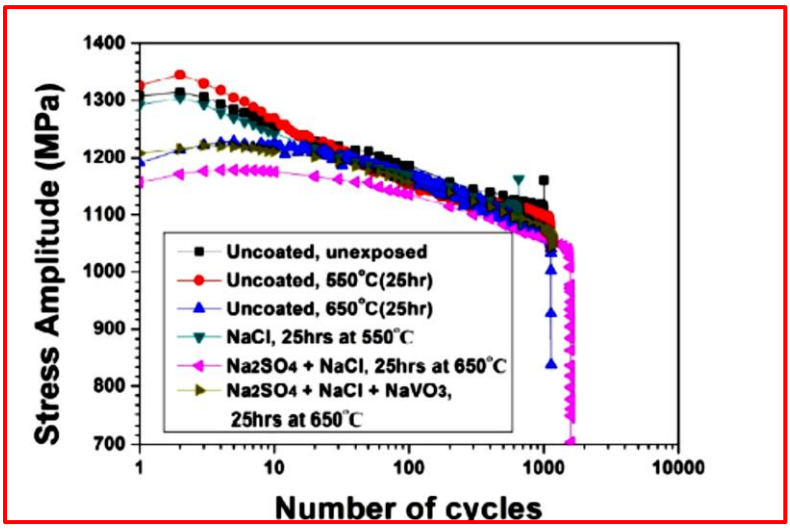

Fig. 1.34: Cyclic stress response curves for the superalloy GTM-SU-718 at room temperature [76].

1.11 Effect of Thermal Barrier Coatings on Low Cycle Fatigue Behaviour

Thermal barrier coatings have received tremendous attention with increase in the demand for higher efficiency through high gas inlet temperatures in gas turbine engine applications. Remarkable combination of high temperature properties can be obtained applying these advanced material systems on substrate material which increases durability of the components and hence reduces the maintenance cost. Due to their low thermal conductivity, TBCs provides insulation and reduces the underneath temperature of the base alloy by almost 80^{o}C to 150^{o}C [22]. These coatings also help in mitigating the uneven temperature distribution effect on the base metal. Typical requirement for an effective TBCs are:

1. Good adherence to the substrate
2. Good insulating capacity i.e. low thermal conductivity
3. High melting point
4. No phase transformation at service temperature
5. Better match of the thermal expansion with the substrate

6. No chemical reaction with the substrate

Though several ceramic materials are available, the above stringent requirements put limitations to the possible materials that can be used in TBC applications. Zirconia (ZrO_2), 8% Yttria Stabilised Zirconia (YSZ), Mullite, Alumina (Al_2O_3), CeO_2, and TiO_2 are some of the ceramic materials available for these applications [77]. Among these YSZ is widely used and studied material because of its better performance at the high temperatures and excellent hot corrosion resistance. Table 1.11 shows comparison of typical properties of the YSZ with Inconel 617 alloy. This material can be used only up to service temperatures of 1200^oC due to its phase transformation above this temperature which may induce cracks in the coating system on exposing to longer durations [77]. Phase transformation occurs from the t′ tetragonal to tetragonal and cubic (t+c) and then to monoclinic (m) [77].

Table 1.11: Comparison of Properties of Inconel 617 Alloy and Yttria stabilized Zirconia (YSZ) [11, 77, 78].

Property	Unit	Inconel 617 Alloy	Yttria Stabilised Zirconia(YSZ)
Melting point	^oC	1330 – 1380	≈2700
Density	gm/cc	8.36	6.05
Modulus of elasticity	GPa	155	205 (40 GPa for Plasma spray coating)
Coefficient of thermal expansion	µm/m-^oC	15.6	10.5
Thermal conductivity	W/m-^oC	1.1	26

Bond coat (BC) is basically applied on the substrate before applying ceramic top coat (TBC), which provides adherence to the top coat material. Bond coat compensate the difference of thermal stresses between the substrate and TBC. It acts as oxidation and corrosion resistant layer to substrate in certain applications. NiCrAlY and NiCoCrAlY are the common bond coat materials, although Ni and Pt aluminides

coatings also sometimes used for this purpose. Bond coats are generally applied using the same processes as used for top coat TBCs. Different methods are available for spraying TBCs on substrates, such as [78, 79],

(i) Electron beam physical vapor deposition (EBPVD),

(ii) Plasma spray methods

   a. Vacuum Plasma Spray (VPS)

   b. Atmospheric Plasma Spray (APS)

   c. Low Pressure Plasma Spray (LPPS)

(iii) High velocity oxygen/ air fuel (HVOF or HVAF),

(iv) Electrostatic spray-assisted vapor deposition (ESAVD), and

(v) Direct vapor deposition

Among the above processes Atmospheric Plasma Spray Process (APS) is the most flexible, economical process and can be widely used with all the commercially available TBC powders. The synthesis of powders in APS process occurs by stacking the lamellae resulting from the impact, flattening, and solidification of the colliding molten powder particles. A strong electric arc is generated between a positively charged pole (anode) and a negatively charged pole (cathode) within the gun which ionizes the gas flowing process gasses (Ar/He and H_2) into the plasma state, which is then forced through a convergent/divergent nozzle [79]. The TBC powder material is injected into the plasma jet which melts the powder particles and propels them onto the substrate material. The molten powder droplets flatten, rapidly solidify and form a deposit as a layer. This process produces high porosity in the coating layer (10-15%) as compared to the other processes such as EBPVD, which is advantageous to some extent, as the pores and cracks existing in the coating provide the tolerance in strains required for strain relaxations that occur during high temperature exposure [77]. APS process is used in the

present investigation to coat TBC of YSZ on to the Inocnel 617 alloy fatigue samples. The details of the material and the method used for ASP process in the present investigation is described in Chapter 2, Section 2.5.3.

Effect of thermal barrier coating of 8%yittria stabilized zirconia on oxidation behaviour of Inconel 617 alloy was studied by Daroonparvar et al. [80]. The TBC was applied on the disc samples of 30 x 5mm using APS process after applying bond coat of NiCr10AlY. Fig. 1.35a shows SEM micrographs of the substrate-BC-TBC interface reveals thickness details. After coating the samples were subjected to oxidation at 1150^{o}C for 18, 22, 26, 32 and 40 h. Thermally grown oxide (TGO) was formed at the interface of BC and TBC, and internal oxidation of BC was also observed after subjecting to oxidation as shown in Fig. 1.35b. Kotowski et al. [81] studied the oxidation resistance of the Inconel 617 alloy coated with YSZ thermal barrier coating. Bond coat was coated by over aluminizing NiCoCrAlY using CVD process. TBC was coated using plasma spray –physical vapour deposition (PS-PVD) method. The oxidation resistance of the alloy was improved due to formation of b-NiAl phase at the substrate-BC interface. The effect of Al_2O_3/Y_2O_3 double layer coating using electrolytic deposition process on oxidation resistance was studied by Hsu et al. [82]. This coating promoted formation of Cr_2O_3 layer by prohibiting formation of NiO which increased oxidation resistance of the alloy. Ebrahimi and Nakhodchi [83] studied the effect of 8% yttria stabilized zirconia (YSZ) thermal barrier coating on thermal fatigue behaviour of Inconel 617 alloy using four point bend test rig. The test rig was designed to simulate the thermal and mechanical conditions of combustor component in a land based gas turbine engine. TBC was applied using APS process. Fig. 1.36 (a) shows the SEM micrograph indicating coating thickness details. They observed temperature gradient of 500^{o}C within the TBC during testing and the surface temperature observed was 1170^{o}C.

The fatigue cracks formed were confined to TBC layer and the TBC system failed after 82 thermal cycles. The final fracture was governed by delamination of the coating at the interface of TBC and BC as shown in Fig. 1.36 (b). Effect of thermal barrier coating on fatigue behaviour of other nickel base super alloys like C263 was studied by Goswami et al. [84] and Fig. 1.37 shows the plot of maximum fatigue stress as a function of cycles to failure at 800^{o}C for TBC coated, substrate with the bond coat and bare Superni C-263. Effect of TBC on LCF studies of 713LC super alloy was studied by Obrtlik et al. [85] and observed the stress response was less in the case of, with TBC samples in comparison with that observed in samples without TBC. However, detailed studies on effect of thermal barrier coating on low cycle fatigue behaviour of Inconel 617 alloy have not been reported so far.

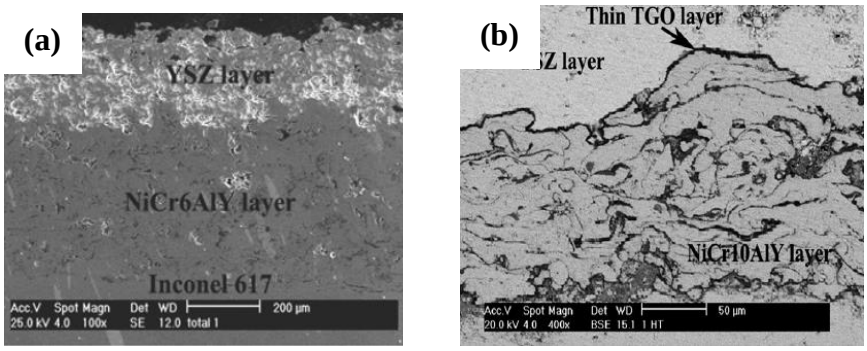

Fig. 1.35: SEM micrographs of the samples (a) after coating with YSZ on base coat of NiCr6AlY and (b) TBC coated samples after subjecting to oxidation at 1150^{o}C for 40 h, showing thin layer of TGO formed [80].

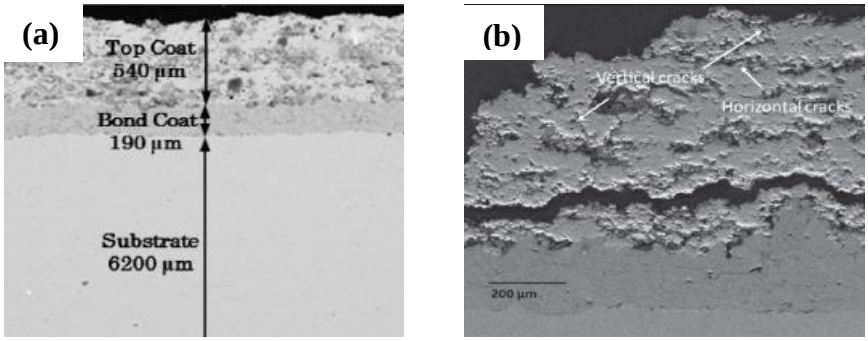

Fig. 1.36: (a) SEM micrograph showing thickness of the bond coat and YSZ coating applied on Inconel 617 alloy (b) micrograph showing cross section of the sample after failure indicating delamination of the TBC layer at the interface of BC and TBC [83].

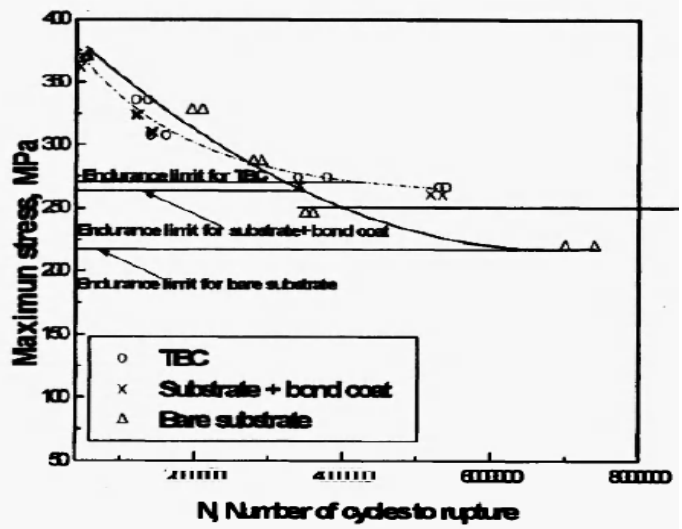

Fig. 1.37: Maximum fatigue stress as a function of cycles to failure at 800^{o}C for TBC coated, substrate with the bond coat and bare Superni C-263 [84].

Application of Inconel 617 alloy in boilers of A-USC power plants requires understanding of the overall mechanical properties and related deformation mechanisms over a wide range of temperatures under tensile, creep and cyclic loading. The primary mode of failure of components made of Inconel 617 alloy is due to cyclic loading (fatigue) resulting from start-up and shut down operations. Temperature induced cyclic strains of different magnitude are also caused by thermal stresses generated during such operations and thus understanding of the low cycle fatigue behaviour and related deformation mechanisms at room temperature as well as at elevated temperatures is necessary. Inconel 617 alloy during its application in combustion lining, is exposed to severe high temperature and corrosive environments. Thermal barrier coating may prove beneficial to improve the life of these alloys at high temperatures, whereas salt environment may be detrimental to the life of these alloys. However, only limited investigations have been carried out on Inconel 617 alloy to evaluate the effect of temperature, microstructure and environment on deformation and fracture behaviour under tensile and fatigue loading both in air and salt environments.

1.12 Scope for the Present Work

Literature survey on Inconel 617 showed that, though attention was paid to understand the controlling mechanisms of DSA in this alloy; however, various manifestations of DSA, characterization of deformation and fracture behaviour under tensile loading had not been examined systematically. DSA has been found to cause deleterious effect on tensile ductility, low cycle fatigue (LCF) life and creep resistance of structural components. Detailed studies on the effect of microstructure on tensile properties and work hardening behaviour of the Inconel 617 alloy are very limited. Also, investigations on the effect of oxidation, salt coating and thermal barrier coating on the LCF behaviour of Inconel 617 alloy at elevated temperatures and their correlations with the deformation and fracture behaviour are scarce. The present investigation was undertaken to address these issues.

1.13 Objectives of the Present Investigation

- To establish the temperature regime of dynamic strain aging for the Inconel 617 alloy based on various manifestations of DSA, deformation and fracture behaviour.
- To carry out detailed investigation on effect of prior material condition on work hardening, deformation and fracture behaviour of Inconel 617 alloy.
- To investigate systematically the low cycle fatigue behaviour of Inconel 617 alloy at different temperatures namely, room temperature, 750°C and 850°C.
- To explore the effect of oxidation, salt coating on low cycle fatigue behaviour of Inconel 617 alloy at 850^{o}C in detail.
- To study the effect of thermal barrier coating on low cycle fatigue behaviour of Inconel 617 alloy at 850^{o}C.